Fachbereich Physik   *Faculty of Physics*
Universität Osnabrück   *Babes-Bolyai University*

Vasile REDNIC

Investigation of electronic and magnetic structure of advanced magnetic materials

Ph.D. Thesis Summary

Scientific supervisors:

Prof. Dr. Manfred NEUMANN   **Prof. Dr. Marin COLDEA**

Osnabrück

January 2010

Contents

Introduction

The problem of local moments confined to the transition metals (T) sites, i.e., localized behaviour in some aspects of itinerant electrons, is one of the most important issues in the physics of the magnetic alloys and intermetallic compounds. It was found experimentally that under certain conditions the magnetic moment of a transition metal remains localized when solute in another transition metal. The condition for the existence of the local moment at the T site is $\pi\Delta / U < 1$, where Δ is the width of the d states (corresponds to the virtual bound states in the Friedel's model) and U is the Coulomb correlation energy between d electrons.

The 3d band width $\Delta = Z^{1/2}J_h$ depends on the number of near-neighbours Z with d orbitals and the hopping integral J_{ohn}, which is very sensitive to the distance between the atoms. On the other hand, the strength and the sign of the interaction between the neighbouring local moments are determined by the occupation fraction of d-orbitals and the orientation of these orbitals in the lattice. By alloying with other elements, the vicinity of the transition metal atom is changing. This leads to structural modifications with remarkable variations in the electronic structure and magnetic properties of the parent compound.

The understanding and prediction of the properties of mater at atomic level represents one of the great achievements of the last years in science. In this content, the advantage of photoelectron spectroscopy, in the study of electronic structure and properties of matter is due to progress in both, experimental and in relevant theory. Photoemission techniques have been developed sufficiently to become a major tool for the experimental studies of solids. These techniques are also attractive for the study of changes in, or destruction of, crystalline order.

The fine details of the relationship between the electronic structure and the magnetic properties of matter represent a state of the art challenge in the solid state physics. The link is evident even from a didactic approach: electrons are the 'carriers' of spin magnetic moments and their movement around nucleus gives rise to orbital momentum i.e. orbital contribution to the magnetic moments. From a more sophisticated point of view, the information on the electronic structure turns up to be essential for the understanding of magnetic behavior.

The XPS spectra give information on the electrons binding energies, the valence band and the density of states at the Fermi level, the hybridization between orbitals, the ions valence states and the charge transfer between the elements. The energy position and the width of the valence band, the comparison between the valence band and the calculated band structure, the splitting of the 3s core level, the presence of the satellite structures to the valence band and 2p core levels give information on the localization degree of the 3d electrons, the occupation of the *3d* band, the spin and valence fluctuations effects, which are the basic elements in explaining the magnetic properties of metallic systems based on 3d elements.

In the present study the ternary system Al-Mn-Ni was chosen because the following reasons:

- Manganese is particularly interesting because according to Hund's rule the magnetic moment of the free atom can have the maximum value of 5 μ_B. The antiferromagnetic alloys formed by Mn with nickel, palladium, and platinum have high Néel temperatures, which makes them very promising materials for practical applications, such as pinning layers of GMR and TMR devices.
- Nickel metal is a ferromagnet having a magnetic moment of 0.6 μ_B/Ni. By alloying with Al, the Ni 3d-Al 3sp hybridization leads to a partial ($AlNi_3$) or complete (AlNi) filling of Ni 3d band depending on Al concentration and distances between Al and Ni atoms.

- By varying the concentration of the elements the first vicinity of transition metal atoms and the distance between them is different, which leads to important changes in the crystallographic and electronic structure with remarkable effects on the magnetic properties of Mn-Ni-Al alloys and compounds.

The aim of this thesis is to study the changes in the crystallographic, electronic and magnetic structure of the Al-Mn-Ni ternary metallic system by modifying the concentration of the constituent elements.

The thesis is organized in 6 Chapters, followed by the summary. Chapter 1 contains a brief theoretical introduction into the magnetism of metallic systems, as well the principles of X-ray photoelectron spectroscopy, which is the main technique used to investigate the electronic structure of the intermetallic alloys and compounds. The sample preparation details and all the experimental techniques employed in the characterization of the systems are described in Chapter 2. The next 4 Chapters contain the experimental results for $Mn_{1-x}Al_xNi_3$, $Mn_{1-x}Al_xNi$, $Ni_{1-x}Mn_xAl$, and $Ni_{0.7-x}Al_xMn_{0.3}$ systems. The structural, electronic and magnetic properties of the alloys and compounds are investigated by X-ray diffraction, X-ray photoelectron spectroscopy, band structure calculations, magnetization and magnetic susceptibility measurements.

Chapter 1. Theoretical Considerations

1.1 General issues of magnetism

The origin of magnetism lies in the orbital and spin motions of electrons and how the electrons interact with one another. The magnetic behavior can be classified into five major groups: Diamagnetism, Paramagnetism, Ferromagnetism, Antiferromagnetism, and Ferrimagnetism. The materials belonging to the first two groups do not exhibit collective magnetic interactions and are not magnetically ordered, while the materials in the last three groups exhibit long-range magnetic order below a certain critical temperature.

At the atomic scale, magnetism comes from the orbital and spin electronic motions. The nucleus can also carry a small magnetic moment, but it is insignificantly small compared to that of electrons. Quantum mechanics gives a fixed energy level to each electron which can be defined by a unique set of quantum numbers: n, l, m_l, and m_s, according to the *Pauli Exclusion Principle*. An electron in an atom goes into an eigenstate having quantitized orbital and spin-angular momenta $\hbar l$ and $\hbar s$, where $h=2\pi\hbar$ is the Planck constant. The magnetic moment of an electron is also quantitized in units of $\mu_B=e\hbar/2mc$, the Bohr magneton, and is given by $m=\mu_B(l+2s)$. The magnetic moment of a free atom (or ion) is the sum of the moments of all electrons. The total angular momentum and the total magnetic moment are given by $\boldsymbol{J=L+S}$ and $\boldsymbol{M}=\mu_B(\boldsymbol{L+2S})=g_J\mu_B\boldsymbol{J}$, respectively, where g_J is the Lande factor. Except for some heavy atoms the Russel-Saunders scheme is valid and the total angular momentum and total spin momentum are $\boldsymbol{L}=\Sigma l$ and $\boldsymbol{S}=\Sigma s$, respectively. When describing the atomic origin of magnetism, one has to consider the orbital and spin motions of all electrons as well as the interactions between them.

1.2 Magnetic properties of metallic systems

In solids, a magnetic moment is exhibited only by an atom with a partially filled *d* or *f* shell. Two series of elements play a fundamental role in magnetism: the *3d* transition elements and the *4f* rare earths. These two series are important because the unfilled shells are not the outer shells and in solids the *3d* (respectively *4f*) shell can remain unfilled, leading to magnetism.

Ferromagnetism of metallic systems based on transition metals has been a controversial subject due to the apparent dual character of the d electrons, i.e., they are itinerant electrons described by band theory in their ground state, while at finite temperatures they show various properties that have long been attributed to a system consisting of local magnetic moments. The most familiar example is the Curie-Weiss law of magnetic susceptibility obeyed by almost all ferromagnets above their Curie temperatures.

The magnetic interaction between localized moments determines the behavior of a compound when placed in a magnetic field and may favor magnetic ordering. The magnetic coupling is usually described in terms of a model spin Hamiltonian, most often the Heisenberg Hamiltonian:

$$H = -\sum_{i,j} J_{ij} \vec{S}_i \vec{S}_j$$

where i, j can be restricted to run over all nearest neighbor or next nearest neighbor pairs of magnetic moments considering that the magnetic interaction is weak and decreases exponentially with distance. Positive values of the constant J correspond to ferromagnetic coupling and negative ones to antiferromagnetic coupling. A spin operator of this form was first deduced from the Heitler-London results by Dirac [1] and first extensively applied in the theory of magnetism by Van Vleck [2]. The universal use of the name Heisenberg Hamiltonian acknowledges his original discussion of the quantum mechanical concept of electron exchange and the introduction of the term *exchange integral* in his theoretical work on the helium atom [3]. When the magnetic orbitals of two neighboring atoms are sufficiently extended to produce a direct overlap, there is an effective interaction between the spins, called *direct exchange.* The origin of the *exchange interaction* is in the different energies for the parallel and antiparallel spin states as a result of the Pauli principle. This direct exchange, which occurs in *3d* intermetallic compounds, is the largest interatomic interaction. When magnetic orbitals of two neighboring atoms are too localized to overlap, as in the case for the *4f* series, the exchange process can occur through conduction electrons if the system is metallic. This leads to the *RKKY indirect exchange interaction.* If there are no conduction electrons, the external electrons of the latter participate in covalent binding and mediate the exchange interaction. This is the *superexchange interaction*, introduced by Kramers [4,5].

Opposite to the localized model is the itinerant (or band) model which considers that each magnetic carrier is itinerant through the solid. In this case, the unpaired electrons responsible for the magnetic moment are no longer localized and accommodated in energy levels belonging exclusively to a given atom, but move in the potential of other electrons and ions, and the corresponding atomic levels form energy bands. The ordered magnetic states, stabilized by electron-electron interactions, are characterized by the difference of the number of electrons with up and down spins. The simplest model of itinerant-electron magnetism is the Stoner model [6], which has mainly been used to account for the existence of ferromagnetism in itinerant systems. If the relative gain in exchange interaction (the interaction of electrons via Pauli's exclusionary principle) is larger than the loss in kinetic energy, the spin up and spin down electron bands will split spontaneously.

Both the localized model and itinerant model fail to fully describe the magnetic behavior of magnetic transition metals. It is very clear that d electrons should be treated as localized electrons in magnetic insulator compounds and as correlated itinerant electrons in transition metals. Theoretical efforts since the 1950s have been concentrated on finding a way of reconciling the two mutually opposite pictures into a unified one, taking into account the effect

of electron-electron correlation in the itinerant electron model. There have been two main directions in this attempt: one was to improve the Stoner theory by considering the electron-electron correlation, and the other was to start with the study of local moments in metals. The picture of local moments in metals resolved the controversy over the two models. A local moment designates a magnetic moment permanently pinned down in a given region in a metallic system where the magnetic electrons, such as the *d* electrons, are not localized. Van Vleck [7] discussed the justification of local moments, considering the importance of electron correlation in narrow *d* bands. An explicit model describing the local moments in metals was proposed by Anderson [8] on the basis of the Friedel picture of virtual bound states in dilute magnetic alloys [9]. The Anderson concept of local moments in metals has been quite important in the development of the theory of ferromagnetic and antiferromagnetic metals. In some cases a metallic ferromagnet can be regarded as consisting of local moments associated with the virtual bound states. Although in this case the local moment is not as well defined as in insulator magnets, an approximate Heisenberg-type picture can be used even in metals. The interaction between local moments in metals was studied by Alexander an Anderson [10] and by Moriya [11] on the basis of the Anderson model. The sign of the interaction between the local neighboring local moments is primarily determined by the occupation fraction of the localized *d*-orbitals [12]:

- when each atomic *d*-shell is nearly half-filled the coupling between the local moments is antiferromagnetic
- when the occupied or empty fraction of each atomic *d*-shell is small the coupling between the local moments is ferromagnetic

These simple rules have been remarkably successful in qualitatively interpreting magnetic properties of a number of magnetic metals, alloys and intermetallic compounds.

1.3 Photoelectron Spectroscopy

Since the original work of Siegbahn and his co-workers [13], photoemission spectroscopy PES has become one of the most important methods for probing the electronic structure of atoms, molecules and condensed matter [14,15]. In a PES experiment, photons from a monochromatized light source are directed on a sample and the photoelectrons liberated by the photoelectric effect are analyzed with respect to emission angle and kinetic energy by an electrostatic analyzer. In photoemission experiments on solids, only electrons originating from a thin surface layer of the sample are normally used in the analysis of the spectra, which makes photoemission a surface sensitive technique. The reason is that only the electrons which leave the sample without loosing energy are carrying information about the electronic structure directly. The large number of electrons which undergo inelastic scattering processes form the secondary electrons background in a photoemission spectrum.

The X-ray photoelectron spectroscopy (XPS) probes the kinetic energies of photoelectrons emitted from inner levels of a solid or from the outermost occupied band, as a result of the interaction of the solid with incoming X-ray radiation of energy $hv > 1000$ eV. In practice, the most used incident X–rays in XPS are Al-K_α (1486.6 eV) and Mg-K_α (1253.6 eV), for which the penetrating power of the photons in a solid is of the order 1−10 micrometers.

Photoelectron emission is a complex process and in consequence there are numerous theoretical theories that try to model it. Modern theories attempt to account for photoemission from a solid in terms of a single unified model, which considers the excitation from an initial state into a damped final state near the surface. However, of great value, is also the traditional

4

three-step model, where the excitation process of the photoelectron, its transport to the surface, and its escape through the surface are considered independently, has been highly successful for low excitation energies.

The experimental quantity measured in XPS is the kinetic energy of the emitted photoelectrons, which allows the determination of the binding energy of each of the emitted electrons. The data are presented as a graph of intensity (usually expressed as counts or counts/s) versus electron energy. The binding energy of the electron is the parameter which identifies the electron specifically, both in terms of its parent element and atomic energy level. Therefore the photoelectron spectrum reproduces the electronic structure of an element quite accurately since all electrons with a binding energy less than the photon energy will feature in the spectrum. The first step which is taken generally in the sample characterization is the recording of a wide scan. This is the so called *survey spectrum*, which allows to identify the chemical components in the sample and to define acquisition windows for the lines which are of interest and will be recorded subsequently with a higher resolution. The electrons which are excited and escape without energy loss contribute to the characteristic peaks in the spectrum, while those which undergo inelastic scattering and suffer energy loss contribute to the *background* of the spectrum. In a XPS survey spectrum we can identify the valence band region at low binding energies (< 20 eV) and the core levels region, as the electrons in an atom can be divided in two categories: core and valence electrons. Core electrons are tightly bound to the nucleus and do not participate directly in the chemical bonding between atoms. Valence electrons, on the other hand, are more loosely bound (low binding energies) and are thus the main contributors in the formation of the chemical bonds. Once a photoelectron has been emitted, the ionized atom must relax in some way. This can be achieved by the emission of an X-ray photon, known as X-ray fluorescence. The other possibility is the ejection of an *Auger* electron. Thus Auger electrons are produced as a consequence of the XPS process.

Chapter 2. Preparation and Characterization techniques

Polycrystalline samples were prepared by arc melting technique in a cold copper crucible under an argon atmosphere. High purity starting materials (>99.99%) were weighted in exact stoichiometric proportions and melted together several times in the same atmosphere. The weight loss of the final samples was found to be less than 1%. The homogeneity of the samples was checked by conventional X-ray powder diffraction. The quality of the samples, in terms of contamination, was also investigated by monitoring the O and C 1s core levels by means of X-ray photoelectron spectroscopy.

The crystallographic structure of all the samples was checked at room temperature using XRD data. The structure investigation of the compounds was performed by conventional X-ray powder diffraction with Cu Kα radiation, using a Bruker AXS D8 Advance powder diffractometer.

The macroscopically magnetic properties were investigated by static and dynamic magnetic measurements in fields up to 10 T and temperature range of 4.2 – 900 K. At low temperatures (below 300 K) a vibrating magnetometer and a SQUID magnetometer were used to measure the spontaneous magnetization of the samples and to determine the Curie temperature and the value of the spontaneous magnetization at 0 K by extrapolation. At high temperatures (above the Curie temperature) the variation of the magnetic susceptibility with the temperature

was obtained using a Weiss balance in the 300 -900 K temperature range and magnetic fields up to 1 T.

The electronic structure of the materials was investigated by means of X-ray photoelectron spectroscopy. The XPS experiments were performed using a commercially available spectrometer PHI Model 5600 Multi-Technique System produced by the Perkin Elmer Corporation, located at the Osnabrück University. The pressure in the UHV chamber was in the 10^{-10}mbar range during measurements.

Theoretical investigations of the electronic and magnetic properties of selected alloys and compounds have been performed using the Munich SPR-KKR package version 3.6 [16]. The electronic structure of the alloys and compounds in the ferromagnetic state were calculated self-consistently by means of the spin polarized relativistic Korringa–Kohn–Rostocker (KKR) method in the atomic sphere approximation (ASA) mode [17,18].

Chapter 3
Electronic structure and magnetic properties of $Mn_{1-x}Al_xNi_3$ alloys [19-21]

This chapter presents the effects of substitution of Al for Mn in $MnNi_3$, investigated by X-ray diffraction, magnetic measurements, X-ray photoelectron spectroscopy (XPS), and band structure calculations. The compounds $MnNi_3$ and $AlNi_3$ are isostructural and crystallize in the $AuCu_3$ structure type. They form solid solutions in the whole range of concentrations.

Earlier studies have shown that the crystallographic disorder degree of $MnNi_3$, defined as the ratio between the Ni sites occupied by the Mn atoms and total number of Mn atoms in the lattice, depends on the preparation method and thermal treatment [22]. The magnetic properties of $MnNi_3$ are strongly influenced by the disorder degree, e.g., the Curie temperatures of ordered and disordered $MnNi_3$ have the values: 770 K and 132 K, respectively [23, 24] and the values of the magnetizations are quite different. In the disordered $MnNi_3$ compound, since the near-neighbour Mn-Mn interactions are antiferromagnetic, a number of Mn magnetic moments do not contribute to the magnetization. As the compound becomes ordered, the ferromagnetic Mn-Ni interactions are dominant and an increase in the magnetization is observed. A fully ordered $MnNi_3$ compound was obtained only after a thermal treatment of 32 days in the 673 K – 828 K temperature range [25]. The magnetic properties of $AlNi_3$ have been of considerable interest since the compound was reported as a Stoner-Wohlfarth weak-itinerant ferromagnet, with T_C = 41.5K [26]. The magnetic properties of $Mn_{1-x}Al_xNi_3$ alloys have been studied only for a limited range of Al concentration, namely for $x \geq 0.7$ [27, 28]. The investigated samples were crystallographically ordered after a thermal treatment at 1323 K for 2 days [28] and at 1123 K for 24 h [27], respectively. It was shown that Al replaces Mn in the crystallographically ordered $Mn_{1-x}Al_xNi_3$ alloys. There is no systematic investigation concerning the magnetic behaviour of the $MnNi_3$ - $AlNi_3$ solid solution system in correlation with XPS measurements.

3.1 Structural characterization

Six samples from the $Mn_{1-x}Al_xNi_3$ system (x=0.0, 0.2, 0.4, 0.5, 0.6, 0.7) were prepared. In order to study the influence of Al on the crystallographic order, no thermal treatment was made after the cooling of the samples. The XRD measurements were performed on polished surfaces, due to the hardness of the samples. The XRD patterns are shown in Fig. 3.1 together with the theoretical spectra of $MnNi_3$ and $AlNi_3$ generated using PowderCell program.

All the investigated alloys are single phases with the same crystallographic structure type as the parent compound MnNi$_3$. The lattice parameters, estimated using the PowderCell program, decreases monotonically with Al concentration from a = 3.5854 Å for MnNi$_3$ to a = 3.5770 Å for Mn$_{0.3}$Al$_{0.7}$Ni$_3$. The lattice parameter of MnNi$_3$ is very close to that reported in literature [29].

3.2 XPS Spectra

XPS valence band spectra of the Mn$_{1-x}$Al$_x$Ni$_3$ alloys and pure Ni are shown in Fig. 3.2. For Al K$_\alpha$ radiation, the Ni 3d cross section is about four times larger than the Mn 3d cross section [30]. Taking also into account the ratio between the contents of Ni and Mn in the alloys, one can say that the valence-bands of Mn$_{1-x}$Al$_x$Ni$_3$ alloys are dominated by the Ni 3d states, which are preponderant at the Fermi level as in metallic Ni. The Mn 3d states are concentrated at the bottom of the valence band in the region around 3 eV binding energy, as was found experimentally and proved by band structure calculations in many alloys and intermetallic compounds based on Mn [31-33]. The XPS valance band spectra of investigated samples present satellite structures at about 6.5 eV, which decreases in intensity with the increase of Al content. The valence band centroids are shifted towards higher binding energies and the density of states (DOS) at Fermi level decreases as the Al concentration increases, suggesting a partial filling of the Ni 3d band due to hybridization of the Al 3sp and Ni 3d states. In d-band metals and alloys the 3d states are shifted gradually to higher binding energy with the increase in the d-state occupancy and consequently a decrease in the density of states at the Fermi level occurs.
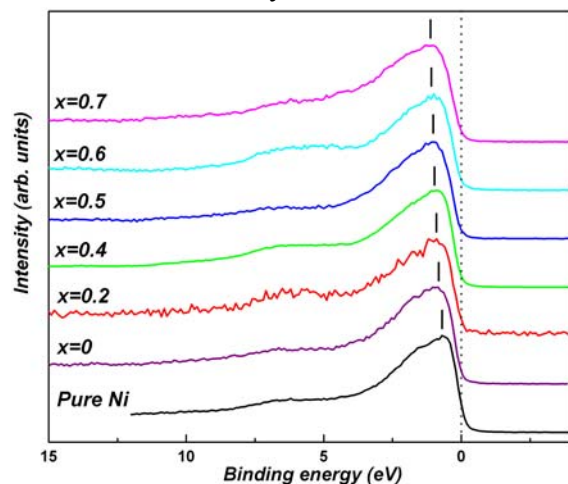

Fig. 3.1. X-ray diffraction pattern of Mn$_{1-x}$Al$_x$Ni$_3$ alloys and the theoretical spectra of MnNi$_3$ and AlNi$_3$

Fig. 3.2. XPS valence band spectra of pure metallic Ni and Mn$_{1-x}$Al$_x$Ni$_3$ alloys. The dotted line and the bars indicate the Fermi level and the position of the valence band centroids

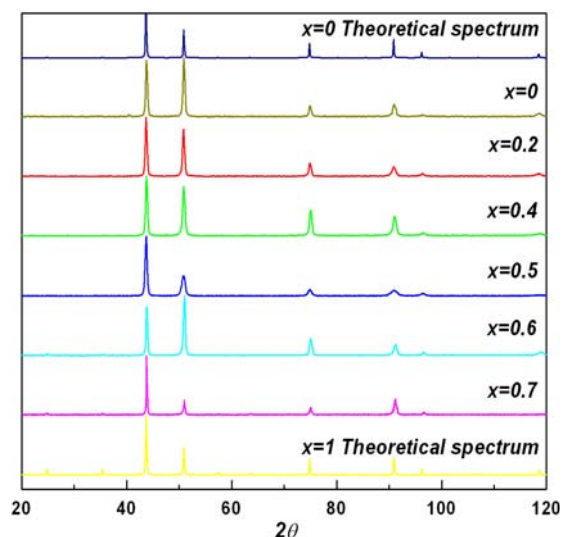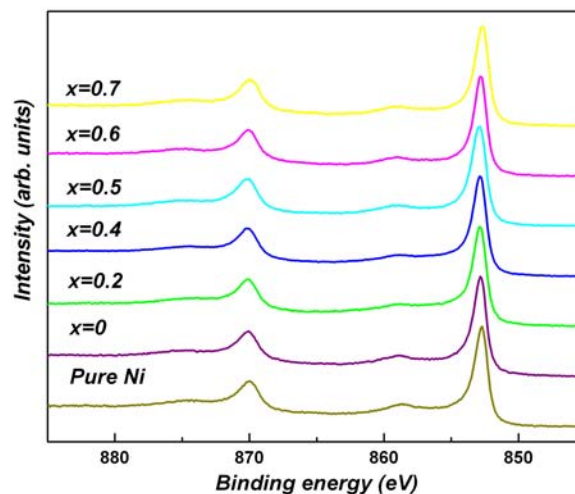Fig .3.3. Ni 2p XPS spectra of Mn$_{1-x}$Al$_x$Ni$_3$ alloys and pure metallic Ni

The Ni 2p XPS spectra of pure metallic Ni and investigated alloys are shown in Fig. 3.3. Like in the case of pure metallic Ni, the Ni 2p$_{3/2}$ core level spectra of Mn$_{1-x}$Al$_x$Ni$_3$ alloys exhibit

satellite structures at about 6.5 eV higher binding energy than the main line. The observation of satellites proves that the Ni 3d band is not completely filled. The relative intensity of the satellite structure is proportional to the unoccupied Ni 3d states and decreases with the Al concentration. This confirms the partial filling of the Ni 3d band due to the hybridization with the Al 3sp states. Similar behavior was observed in other Ni alloys [34].

There is an overlapping between Mn2p XPS line and Ni $L_2M_{23}M_{45}$ Auger line (Fig. 3.4).
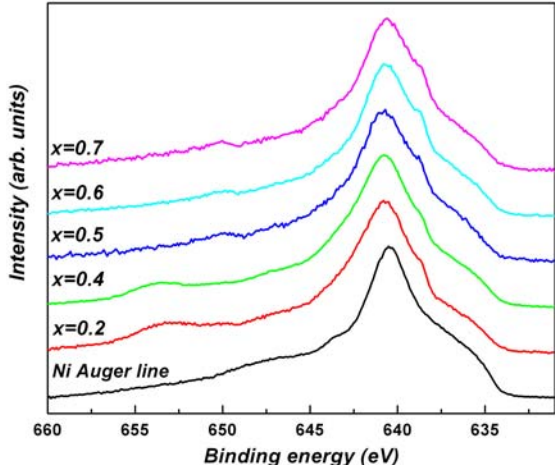
Fig .3.4 Mn 2p XPS spectra of $Mn_{1-x}Al_xNi_3$ alloys before the subtraction of the Ni Auger Line	Fig .3.5. Mn $2p_{3/2}$ curve fitting results of $Mn_{0.3}Al_{0.7}Ni_3$ alloy
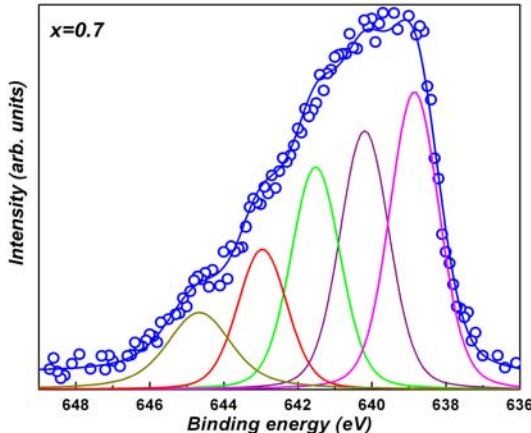
After the Ni Auger line subtraction and background removal, using a Shirley-type background shape, we have also fitted the Mn $2p_{3/2}$ core-level spectra for some of the investigated alloys with four components and a satellite line situated at binding energy around 644.5 eV. The curve fitting results for $Mn_{0.3}Al_{0.7}Ni_3$ is given in Fig. 3.5, with the mean energy separation $\Delta_{ex} \approx 1.1$ eV. This is a clear evidence of the existence of local moments confined on Mn sites.

3.3 Magnetic measurements

The values of the spontaneous magnetization, for each temperature, were determined from M(H) curves by extrapolation the linear dependence at H→0. The temperature dependence of the spontaneous magnetization of $Mn_{1-x}Al_xNi_3$ alloys is shown in Fig. 3.6.
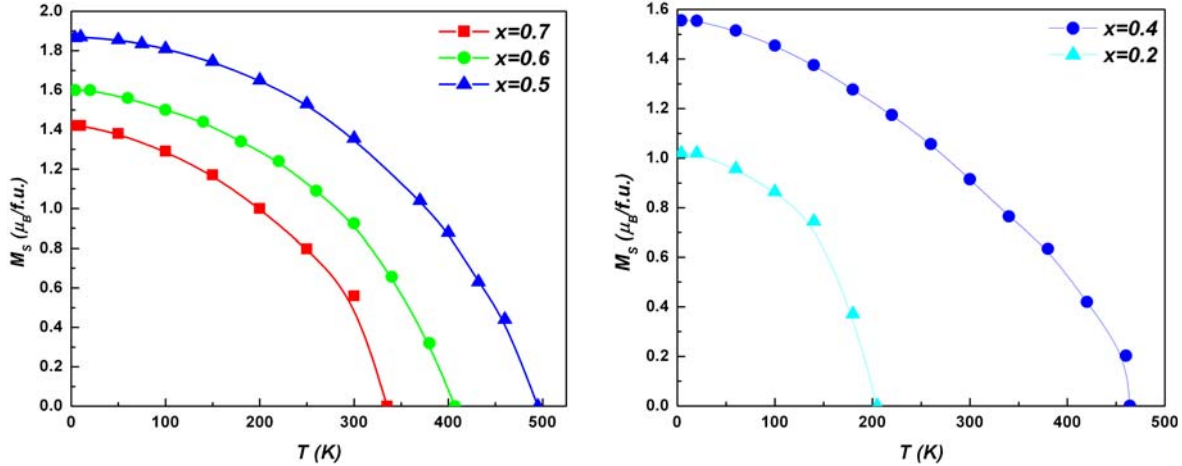

Fig. 3.6. Temperature dependence of spontaneous magnetization of $Mn_{1-x}Al_xNi_3$ alloys

The variation of magnetization with temperature suggests that the investigated alloys have a ferromagnetic behavior, below the corresponding Curie temperatures. Nevertheless, the values of the spontaneous magnetizations show that for high Mn concentrations appear Mn-Mn

antiferromagnetic pairs which lead to smaller values of the spontaneous magnetization per unit formula.

Fig. 3.7 shows the temperature dependence of the reciprocal susceptibility of $Mn_{1-x}Al_xNi_3$ alloys in the paramagnetic state. In the high temperature range the magnetic susceptibilities of all investigated samples obey the Curie-Weiss law, $\chi = C / (T-\theta)$. The magnetic susceptibility of ferrimagnetic materials follows a Néel-type hyperbolic law. However, the high temperature asymptote to the hyperbola is of Curie-Weiss form.

The transition Curie temperatures (determined from the Arrot plots), the paramagnetic Curie temperatures and magnetic moments both in the ordered and paramagnetic state are given in Table 3.1.
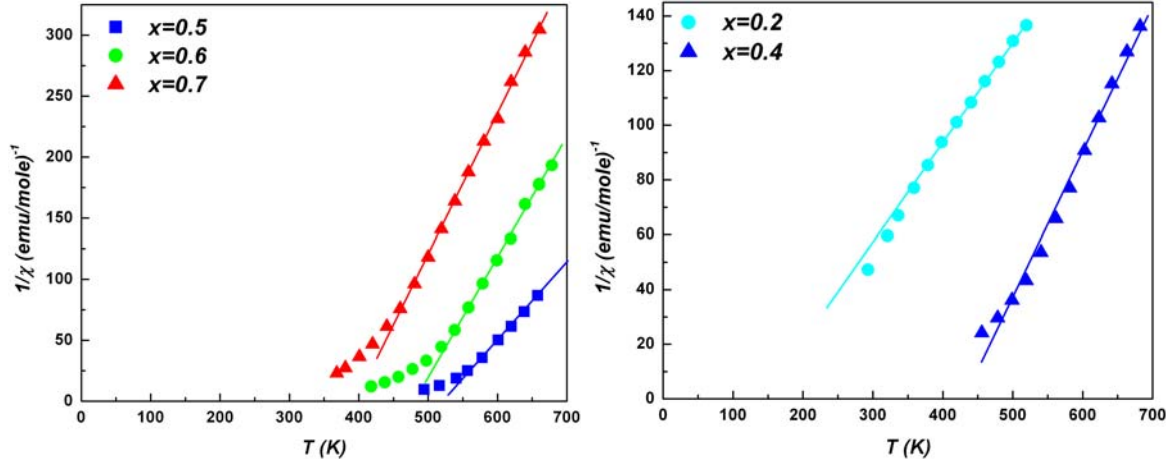

Fig. 3. 7. Reciprocal susceptibility versus temperature of $Mn_{1-x}Al_xNi_3$ alloys

Table 3.1. Curie temperatures T_c , paramagnetic Curie temperatures θ, magnetic moments in the ordered magnetic state (μ_s) and paramagnetic state (μ_{eff}) of $Mn_{1-x}Al_xNi_3$ alloys

Compound	T_C (K)	μ_s (μ_B/f.u.)	θ (K)	μ_{eff} (μ_B/f.u.)
$Mn_{0.8}Al_{0.2}Ni_3$	205	1.02	137	4.7
$Mn_{0.6}Al_{0.4}Ni_3$	464	1.56	426	3.9
$Mn_{0.5}Al_{0.5}Ni_3$	495	1.86	518	3.6
$Mn_{0.4}Al_{0.6}Ni$	407	1.6	477	2.9
$Mn_{0.3}Al_{0.7}Ni_3$	335	1.42	397	2.6

In Fig. 3.8, the values of the Curie temperature T_C and paramagnetic Curie temperature θ obtained in the present work are plotted together with the values of T_C from earlier magnetic measurements, versus Al content for $Mn_{1-x}Al_xNi_3$ alloys. There is a good agreement between our results concerning the Curie temperatures T_C for $x \geq 0.5$ and those reported earlier on crystallographically ordered samples. On the other hand, the Curie temperatures for $x < 0.5$ are smaller than the expected values for ordered alloys (the upper broken line in Fig. 3.8). These results suggest an increase in the crystallographic ordering of $Mn_{1-x}Al_xNi_3$ alloys as the Al content increases. The monotonic decrease of T_C with Al concentration in the ordered state may be explained by the reduction of the number of ferromagnetic Mn - Ni pairs. On the contrary, in the disordered state T_C increases with Al content due to the decrease in the number of antiferromagnetic Mn - Mn pairs. The paramagnetic Curie temperatures θ for ordered alloys are higher than the transition Curie temperatures T_C, as is expected for a ferromagnetic material, while in the disordered state,$\theta < T_C$, characteristic for a ferrimagnetic behaviour.

9

The correlation of XPS data and magnetic measurements for ordered and paramagnetic states suggests the existence of local magnetic moments on the Mn and Ni sites in $Mn_{1-x}Al_xNi_3$ alloys. The compound $AlNi_3$, which is known as a spin fluctuation system, has the Ni 3d band almost filled with a magnetic moment in the ordered state of $\mu=0.075\ \mu_B$/Ni [35]. The Mn and Ni magnetic moments in $MnNi_3$ compound, both in ordered and disordered crystallographically state, have the values of 3.2 μ_B and 0.3 μ_B, respectively [25,36]. The band structure calculations on ferromagnetic $Ni_{0.5}Mn_{0.5-x}Al_x$ alloys have
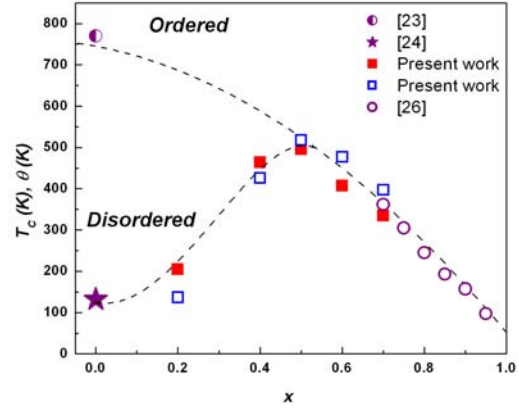

Fig. 3.8. Curie temperatures T_C and paramagnetic Curie temperatures θ of $Mn_{1-x}Al_xNi_3$ alloys as a function of Al content. The broken lines are guides for the eyes.

shown that the hybridization between the Mn 3d and Al 3sp states is very low and the Mn magnetic moment is not affected by the presence of Al atoms in the lattice [37]. One can assume that the Mn magnetic moment in $Mn_{1-x}Al_xNi_3$ alloys has approximately the same value of 3.2 μ_B as in the parent compound $MnNi_3$. On the other hand, the Ni magnetic moment in Ni-Al alloys decreases linearly with the Al content in the range of solid solubility [38]. With this assumption, when the Al concentration in $Mn_{1-x}Al_xNi_3$ increases, the magnetic moment of Ni atom in the ordered magnetic state would linearly decrease from 0.3 μ_B/Ni in $MnNi_3$ to 0.075 μ_B/Ni in $AlNi_3$. This is also confirmed by our XPS measurements. The disorder degree D in $Mn_{1-x}Al_xNi_3$ alloys can be calculated in this way from the values of the magnetic moments in the ordered magnetic states μ_s. In the paramagnetic state, one can estimate the effective magnetic moment of Ni atoms from the Curie constant, $C_{f.\ u} = C_{Mn} + C_{Ni}$. In Table 3.2 are given the estimated values of the disorder degree and the magnetic moments per Ni atom both in the ordered (μ_s^{Ni}) and paramagnetic state (μ_{eff}^{Ni}).

Table 3.2. Disorder degrees D (%) and magnetic moments of Ni atoms in the ordered state (μ_s^{Ni}) and paramagnetic state (μ_{eff}^{Ni}) of $Mn_{1-x}Al_xNi_3$ alloys

Compound	$Al_{0.2}Mn_{0.8}Ni_3$	$Al_{0.4}Mn_{0.6}Ni_3$	$Al_{0.5}Mn_{0.5}Ni_3$	$Al_{0.6}Mn_{0.4}Ni_3$	$Al_{0.7}Mn_{0.3}Ni$
D (%)	45	15	10	7	0
μ_s^{Ni} (μ_B)	0.25	0.21	0.19	0.16	0.14
μ_{eff}^{Ni} (μ_B)	1.70	1.32	1.23	0.75	0.74

The inequality $p_c > p_s$ between the numbers of spins per Ni atom in the paramagnetic state p_c and ordered magnetic state p_s is valid for all investigated alloys and the ratio p_c / p_s decreases with the Al content. We may explain the contribution of Ni atoms to the measured susceptibility in $Mn_{1-x}Al_xNi_3$ alloys in terms of the self-consistent renormalization theory of spin fluctuations [35]. This theory has revealed that only a small-q part of the wave-number-dependent susceptibility χ_q contributes to the temperature dependence of χ in nearly ferromagnetic metals (exchange-enhanced Pauli paramagnets). The average amplitude of the local spin fluctuations on Ni sites $< S_L^2 >= 3k_B T \sum_q \chi_q$ increases with temperature until it reaches an upper limit determined by the charge neutrality condition. The temperature dependence of χ at low temperatures is the result of the increase of local moments with increasing temperature. The

amplitude $<S_L^2>$ of thermally excited longitudinal spin fluctuations saturates at certain temperature T* above which the susceptibility is governed by local moment type fluctuations and therefore a Curie-Weiss behaviour is observed. The partial filling of the Ni 3d band with the increase of Al concentration leads to a decrease of the spin fluctuations amplitude and consequently a reduction of the ratio p_c / p_s is observed.

3.4 Electronic structure calculations

In the following pages are presented the Band structure calculations of $Mn_{1-x}Al_xNi_3$ alloys ($0 \leq x \leq 0.8$) in order to evidence the effects of the Mn substitution by Al on the local Mn and Ni magnetic moments and to compare these values with the experimental ones. The disorder degree influence on the magnetic moments of the $Mn_{1-x}Al_xNi_3$ alloys is also investigated. The XPS valence band spectra and the density of states were calculated and compared to the experimental results.

Band structure calculations in ferromagnetic spin configuration (with all Mn and Ni magnetic moments parallel) have been performed for $Mn_{1-x}Al_xNi_3$ alloys in order to determine the dependence of the magnetic moments on the disorder degree and the Al content. The variation of Mn and Ni magnetic moments with the Al content is presented in Fig. 3.9.

The magnetic moments of Mn and Ni on their proper sites (1a and 3c, respectively) are different affected by the Mn substitution with Al and by the disorder degree in the system, respectively. We expect that the decrease of the magnetic moments of Ni 3c with Al content is a
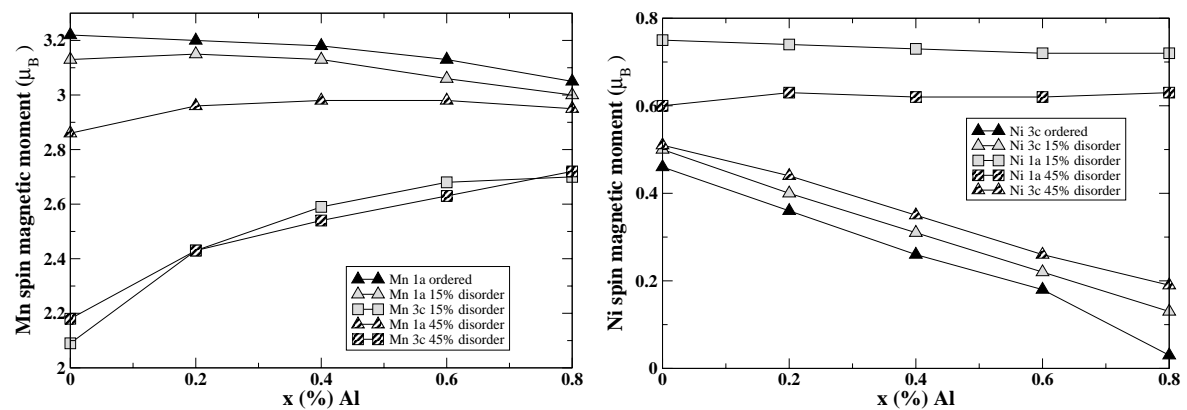

Fig.3.9. Calculated magnetic spin moments of Mn and Ni atoms in $Mn_{1-x}Al_xNi_3$ alloys, using different disorder degrees.

The Mn magnetic moments are smaller when Mn atoms are on antisites due to the decrease of Mn-Mn distance ($d_{Mn1a-Mn3c} \approx 2.53$ Å), which leads to the increase of the delocalization degree of the Mn 3d electrons. The 3d band width $\Delta \approx Z^{1/2}J_h$ depends on the number of near-neighbours Z with d orbitals and the hopping integral J_h, which is very sensitive to the distance between the atoms. In case of Mn (3c) atoms the number of near-neighbours having d orbital decreases when Al concentration increases. This means that the 3d band becomes narrower, 3d electrons are more localized, and all these leads to an increase of Mn magnetic moment.

Also, the Ni magnetic moment on antisite is much higher than the Ni sitting on the proper site but is less influenced by the Al content. This could be assign to the fact that Ni 1a atoms do not have Al atoms in their first vicinity. In the case of $Mn_{0.8}Al_{0.2}Ni_3$ alloy, with high D values, there is a significant influence of the disorder degree on the Ni 1a magnetic moment (Fig.3.9).

11

The orbital magnetic moment is not completely quenched by the crystal field, but his contribution to the total magnetic moment is very small.

The Mn and Ni magnetic moments in the $Mn_{1-x}Al_xNi_3$ alloys, using the disorder degree D determined by experiment, were calculated. The calculated total magnetic moment per unit cell, using the experimental determined disorder degrees is in reasonable agreement with the magnetic moment per unit cell determined from magnetization measurements, only for $x \geq 0.5$. The change of the disorder degree in the theoretical calculations doesn't improve this agreement. The measured values of the magnetic moments per unit cell for $x \leq 0.4$ are much smaller than those predicted by the ferromagnetic spin configuration, confirming the existence of Mn-Mn pairs antiferromagnetically coupled, in good agreement with experimental results.

The XPS valence band spectra were also calculated in order to allow a direct comparison of the computed and experimental XPS valence band spectra (Fig. 3.10). The XPS valence band spectra for all $Mn_{1-x}Al_xNi_3$ alloys and compounds are dominated by the Ni 3d states. The Mn contribution to the XPS spectra has a maximum at about 4 eV binding energy, which is visible in some of the spectra by a shoulder in the total intensity. The satellite structures at about 6.5 eV are caused by the enhanced electron correlation in the Ni 3d band, providing an evidence for the unoccupied states in the Ni 3d band. The correlation effects have not been implemented in the theoretical framework and this feature is absent in the theoretical spectra. The calculated XPS valence band spectra describe the main characteristics of the experimental ones. The contribution of the Mn 3c and Ni 1a in the calculated XPS valence band spectra for x>0.6 is negligible because
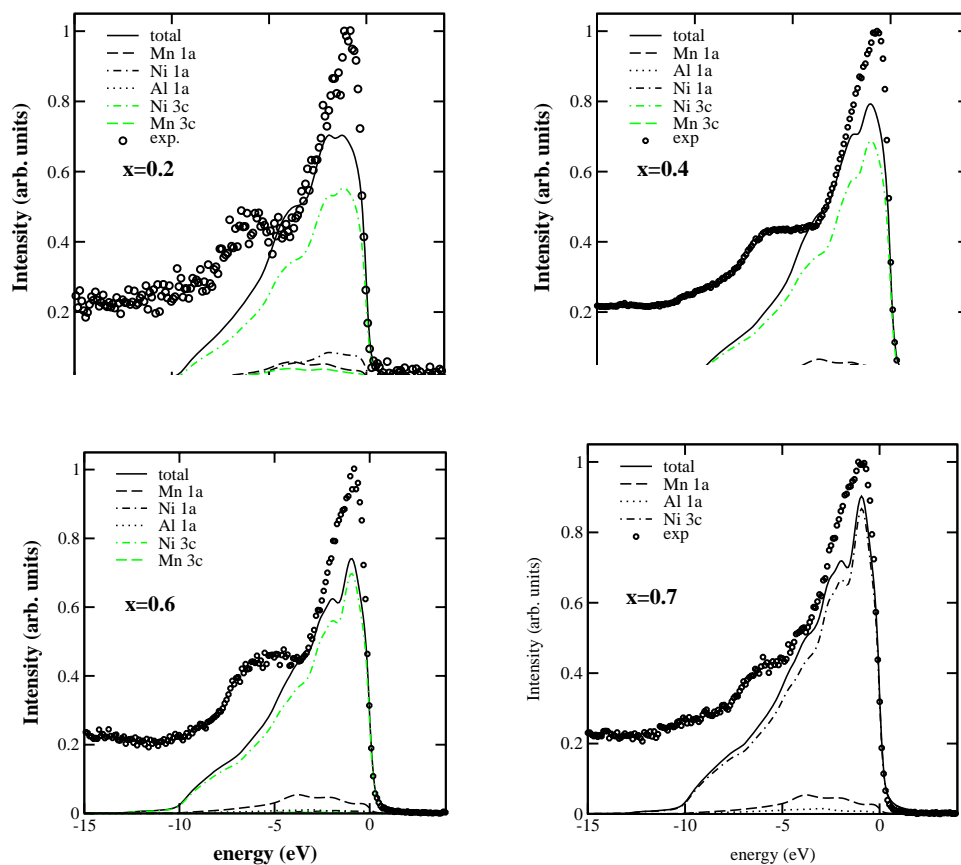

Fig.3.10. Calculated (lines) and experimental (circles) XPS valence band spectra of $Mn_{1-x}Al_xNi_3$ alloys for x = 0.2, 0.4, 0.6 and 0.7.

The total DOS calculations for investigated alloys are presented in Fig. 3.11. On can see that there are no changes on the DOS at Fermi level in the spin-up band but there is a significant decrease of DOS in the spin-down band when Al concentration increases, suggesting a partial filling of the Ni 3d band due to the hybridization between Ni 3d and Al 3sp states.
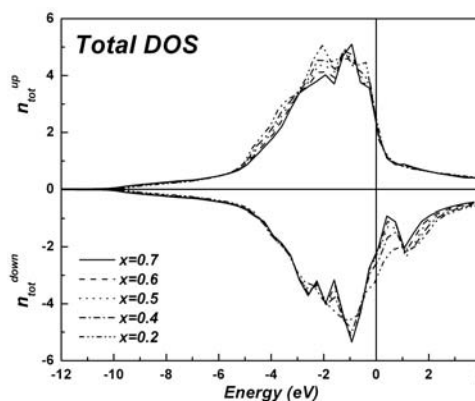

Fig.3.11. Total spin resolved DOS of $Mn_{1-x}Al_xNi_3$ alloys

Chapter 4
Electronic structure and magnetic properties of $Mn_{1-x}Al_xNi$ alloys [39]

MnNi has one of the highest Néel temperature (T_N =1073K), a magnetic moment of 4 μ_B/Mn [40] and is used in the spin electronic devices as a pinning layer in the spin-valve structures [41]. AlNi is a Pauli paramagnet with the Ni 3d band completely filled at room temperature [42]. The magnetic properties of $Mn_{1-x}Al_xNi$ alloys have been studied only for a limited range of Al concentration, namely for x=0.4 [43, 44] and 0.5 [45]. For $MnAlNi_2 \equiv Mn_{0.5}Al_{0.5}Ni$ Heusler alloy was pointed out the coexistence of antiferromagnetism and ferromagnetism [45]. The $Mn_{0.6}Al_{0.4}Ni$ alloy, thermal treated for three days at 1273 K, exhibits the B2-10M martensitic transformation [44]. It was also shown that in the furnace-cooled specimen of the $Mn_{0.6}Al_{0.4}Ni$ alloy, the $L2_1$ structure appears and the B2-10M martensitic transformation is suppressed.

The aim of this chapter is to extend the magnetic measurements to whole range of concentrations and to correlate the magnetic data with XPS spectra.

4.1 Structural characterization

Nine samples from the $Mn_{1-x}Al_xNi$ system (x= 0, 0.1, 0.2, 0.4, 0.5, 0.6, 0.8, 0.9, 1) were prepared. XRD measurements revealed a change in the crystallographic structure around x = 0.4 from CuAuI to CsCl (B2) structure type. In Fig. 4.1 are shown the XRD patterns for all investigated samples. $Mn_{0.6}Al_{0.4}Ni$ appears as a mixture of these two structures.

The B2 phase has the same structure with the $L2_1$ phase of Heusler alloys, having the unit cell equals with the 8-th part from the last one. In the B2 phase of $Mn_{1-x}Al_xNi$ alloys, the Mn and Al atoms
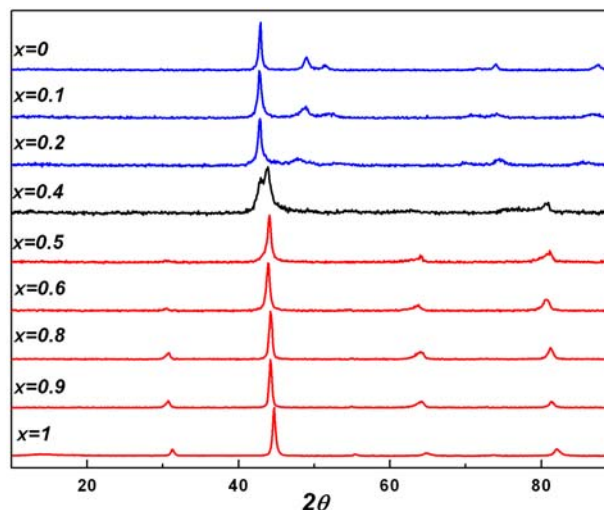

Fig. 4.1. X-ray diffraction pattern of $Mn_{1-x}Al_xNi$ alloys.

are randomly arranged, thus the near-neighbor Mn-Mn distance is about 0.29 nm. In the $L2_1$ structure, where the Mn atoms are separated by Al atoms, the shortest Mn-Mn distance is 0.41 nm.

4.2 XPS Spectra

The Mn 3s spectra for MnNi, $Mn_{0.9}Al_{0.1}Ni$ and $Mn_{0.8}Al_{0.2}Ni$ are shown in Fig. 4.2. The shoulder around 79 eV corresponds to the Ni 3p satellite situated at about 12 eV higher binding energy from the main line [46].
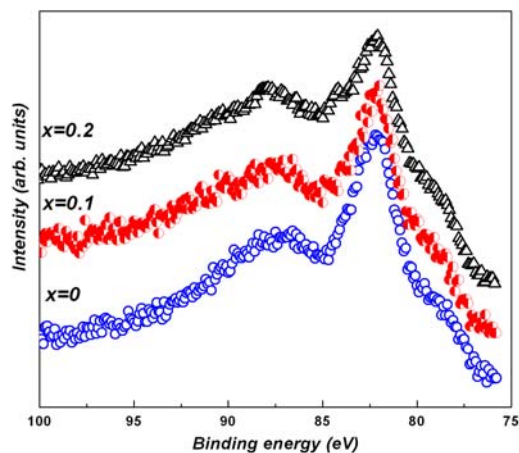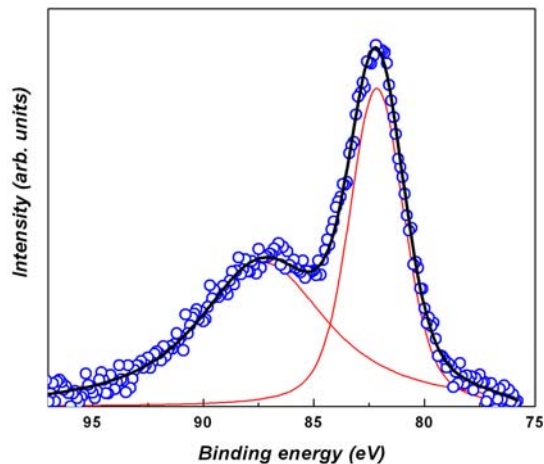

Fig. 4.2. Mn 3s XPS spectra of $Mn_{1-x}Al_xNi$ alloys

Fig. 4.3. Mn 3s curve fitting results of MnNi compound

Fig. 4.3 presents the curve fitting results of MnNi compound, after background and Ni 3p satellite subtraction. Similar results were obtained for the other two alloys $Mn_{0.9}Al_{0.1}Ni$ and $Mn_{0.8}Al_{0.2}Ni$. All spectra exhibit a well-defined magnetic exchange splitting of about 5 eV. This splitting corresponds to a spin S≈2 and a magnetic moment of $4\mu_B$/Mn, suggesting that Mn 3d band is not affected by the hybridization with Al sp states. This splitting is a direct evidence for the existence of local magnetic moment confined on Mn sites.

There is an overlapping between Mn2p XPS line and Ni $L_2M_{23}M_{45}$ Auger line (Fig. 4.4). In order to see the multiplet splitting of Mn $3p_{3/2}$ line the Auger line was subtracted (Fig. 4.5).
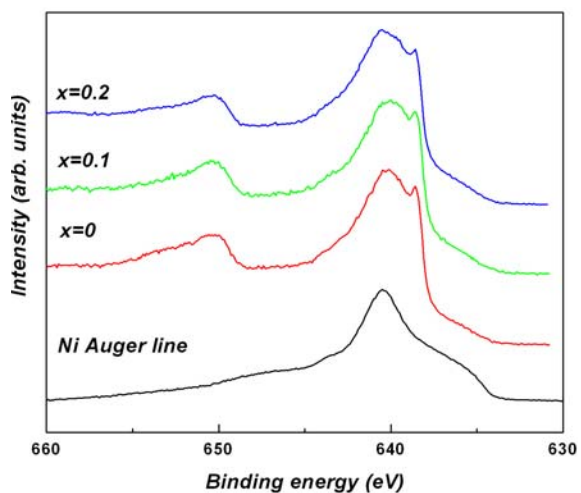

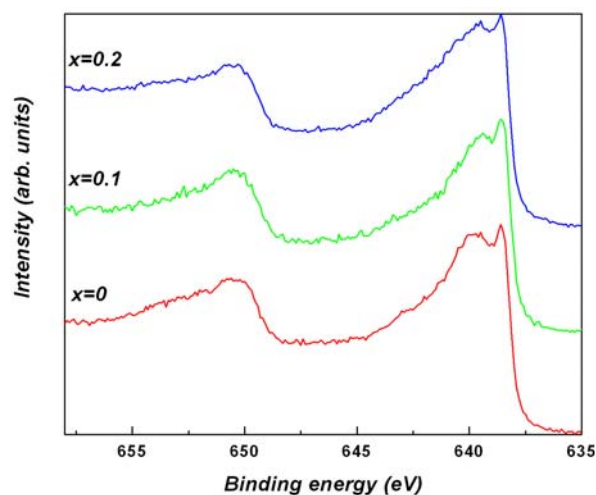Fig. 4.4. Mn 2p XPS spectra of $Mn_{1-x}Al_xNi$ alloys and Ni Auger line

Fig. 4.5. Mn 2p XPS spectra of $Mn_{1-x}Al_xNi$ alloys after the subtraction of the Ni Auger Line

14

The first vicinity of Mn atoms in the $Mn_{1-x}Al_xNi$ alloys does not change by alloying, what explains the lack of the chemical shift in the Mn 2p spectra.

We have also fitted the Mn $2p_{3/2}$ core-level spectra for some of the investigated alloys like in the previous chapter. The mean energy separation was $\Delta_{ex}\approx1.1$ eV. This gives further evidence of the existence of local moments confined on Mn sites.

The Ni 2p core-level spectra of $Mn_{1-x}Al_xNi$ alloys are shown in Fig. 4.6. The Ni $2p_{3/2}$ core level spectra for x≤0.8 exhibit satellite structures situated at about 6.5 eV higher binding energy than the main line. The observation of satellites implies the presence of d character in the unoccupied bands. The satellite structure intensity decreases as the Al content increases, indicating a gradual filling of the Ni 3d band due to a strong hybridization with Al 3sp states.
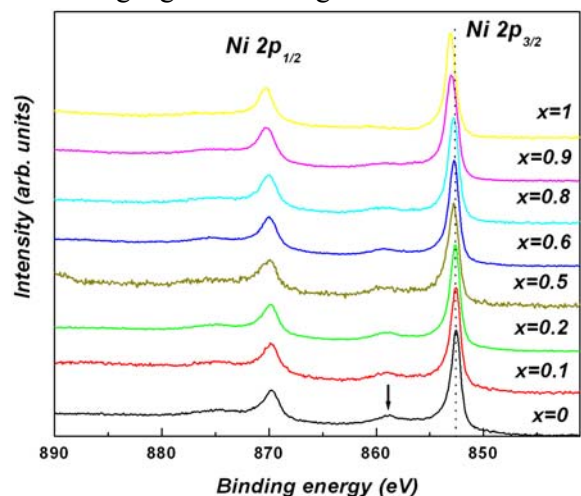

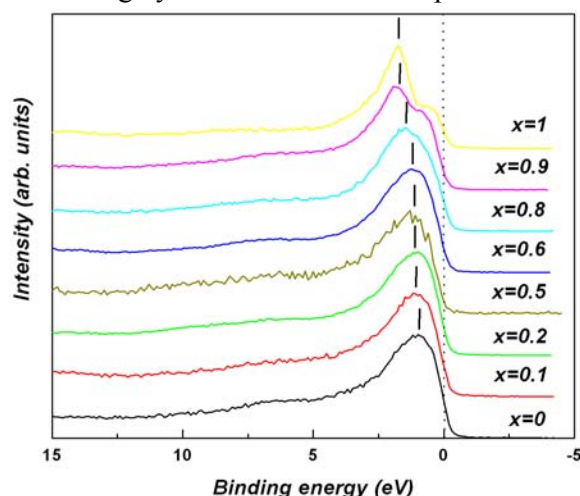*Fig .4.6. Ni 2p XPS spectra of $Mn_{1-x}Al_xNi$ alloys*   *Fig .4.7. XPS valence band spectra of $Mn_{1-x}Al_xNi$ alloys*

The complete filling of the Ni 3d band, at room temperature, for AlNi Pauli paramagnet is confirmed by the absence of the satellite structures. This behavior was also observed in other Ni alloys [47]. The presence of the satellite structures suggests that Ni atoms could carry a small magnetic moment, but previous studies have shown that in MnNi the Ni atoms have no magnetic moments [48]. This means that even in the presence of some unoccupied states in the Ni 3d band the Anderson condition for the existence of the local moment at the Ni site in the ordered magnetic state is not fulfilled. As the Al concentration increases, the Ni 2p core-level lines are shifted to higher binding energy. These small chemical shifts are due to the change in the filling degree of the Ni 3d band, which leads to an increase in the electronic density around the Ni 2p shell.

The XPS valence band spectra of $Mn_{1-x}Al_xNi$ alloys are shown in Fig. 4.7. The valence band of Pauli paramagnet AlNi results as a superposition of the Ni 3d band, centered at about 2 eV, and the Al sp states in the Fermi level region. The XPS valance band spectra of investigated samples present a small satellite structures at about 6.5 eV, which decreases in intensity with the increase of Al content. The 3d bands are shifted towards higher binding energies as the Al concentration increases, suggesting a gradual filling of the Ni 3d band.

4.3 Magnetic measurements

Since the Ni atoms do not carry any magnetic moment [45, 48], the interaction Mn-Mn is responsible for the magnetic properties of all investigated alloys. The alloys $Mn_{1-x}Al_xNi$ for x<0.4 are antiferromagnets with very high Néel temperatures, namely 1073 K for MnNi [40], 1026 K for $Mn_{0.9}Al_{0.1}Ni$ and 820 K for $Mn_{0.8}Al_{0.2}Ni$. For illustration, in Fig. 4.8 is shown the temperature

dependence of the measured magnetic susceptibility for $Mn_{0.9}Al_{0.1}Ni$ alloy. The distance between the nearest-neighbor Mn atoms in these alloys, determined from XRD measurements, is about 2.64 Å. It is well known that the Mn-Mn interaction is antiferromagnetic when the distance is smaller than 3 Å [49].

The magnetic field dependence of magnetization at different temperatures for $x \geq 0.5$ shows a small curvature (Fig. 4.9), suggesting the presence of a ferromagnetic phase $L2_1$, in which the interaction between the Mn atoms is due to the RKKY coupling [50]. On the other hand, the magnetization does not saturate even at B=10 T, what implies the existence in the alloys of the antifferromagnetic B2 phase.

The alloys $Mn_{1-x}Al_xNi$ for $0.4 < x < 1$ have complex mictomagnetic behavior, with a mixture of antiferromagnetic and ferromagnetic interactions. The coexistence of antiferromagnetism and ferromagnetism in
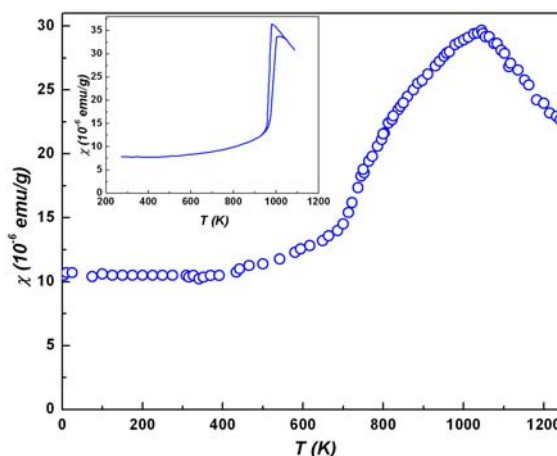

Fig.4.8. Susceptibility versus temperature of $Mn_{0.9}Al_{0.1}Ni$ alloy. In the inset is shown the thermal variation of the susceptibility for MnNi [40].

$Mn_{0.5}Al_{0.5}Ni$ alloy was also confirmed in the literature by the susceptibility measurements in field cooled (FC) and zero field cooled (ZFC) [45].
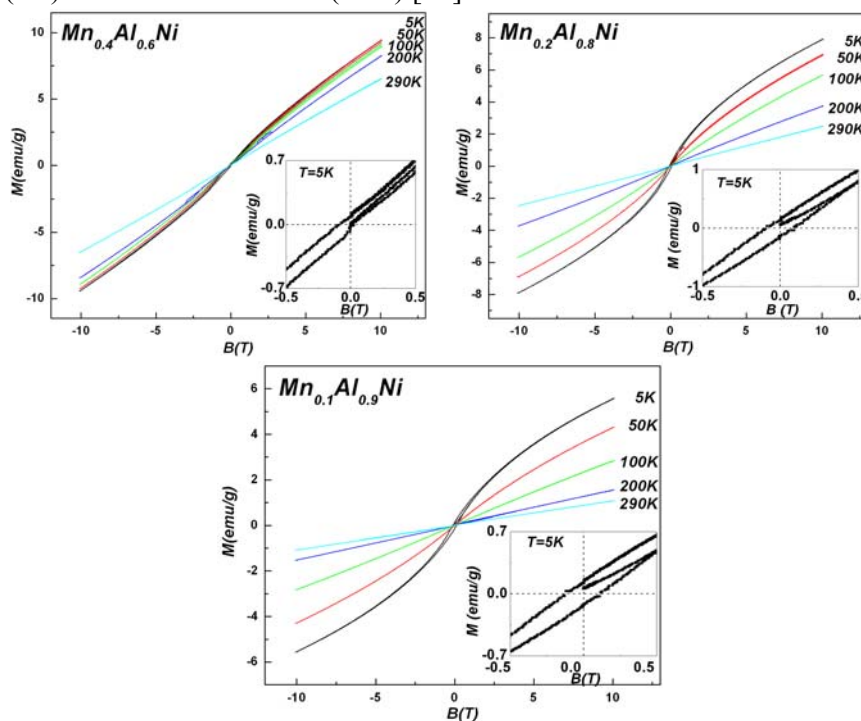

Fig.4.9. Magnetic field dependence of magnetization, at different temperatures, of $Mn_{0.4}Al_{0.6}Ni$, $Mn_{0.2}Al_{0.8}Ni$ and $Mn_{0.1}Al_{0.9}Ni$ alloys.

The hysteresis loops (see the insets) are shifted to lower negative fields, the effect being more pronounced for x=0.6. The shift in the magnetization of a ferromagnetic component is due to the exchange interaction between the antiferromagnet and ferromagnet at their interface. The ferromagnetic component, which is strongly coupled with the antiferromagnetic one, has its

interfacial spins pinned. At lower Mn concentrations, i. e. x = 0.8 and x = 0.9, the amount of antiferromagnetic component decreases (the probability to have Mn-Mn pairs becomes smaller), what explains the almost symmetrical form of the hysteresis loop in this concentration range. The coercive field at T = 5 K increases as Mn concentration decreases, from 0.05 T for x = 0.6 to 0.11 T for x = 0.9. The small values of the coercive field can be explained in the random anisotropy model [51]. The increase of the coercive field as temperature decreases indicates enhancement of the local magnetic anisotropy.

The coexistence of antiferromagnetism and ferromagnetism in $Mn_{1-x}Al_xNi$ alloys for 0.6 ≤ x < 1 is also revealed by the magnetic measurements in lower magnetic fields. In fig. 4.10 is shown the temperature dependence of FC and ZFC susceptibilities in an applied field of 0.1T. The distinguishing experimental feature of mictomagnetism is that the magnetization drops abruptly at the freezing temperature T_f when the material is cooled in the absence of magnetic field, resulting in a splitting of the FC and ZFC susceptibilities at a certain temperature. The values of this temperature and also the freezing temperature are related to the dilution effect, like in other mictomagnetic systems [52]. The exchange interactions of Mn-Mn type are partially broken when Mn is substituted by Al. The increase of the ZFC susceptibility for x = 0.6 at low temperatures was also observed for x=0.5 [45] and may be due to the conical antiferromagnetic structure of B2 phase, which has a ferromagnetic component. This conical antiferromagnetic structure was observed in the B2 phase of $MnAlNi_2 \equiv Mn_{0.5}Al_{0.5}Ni$ compound [53].

Fig. 4.10. The temperature dependence of the FC and ZFC magnetic susceptibility of $Mn_{1-x}Al_xNi$ alloys.

In order to determine the ferromagnetic (FM) and antiferromagnetic contributions to the measured magnetization and to estimate the corresponding Curie and Néel temperatures T_C and
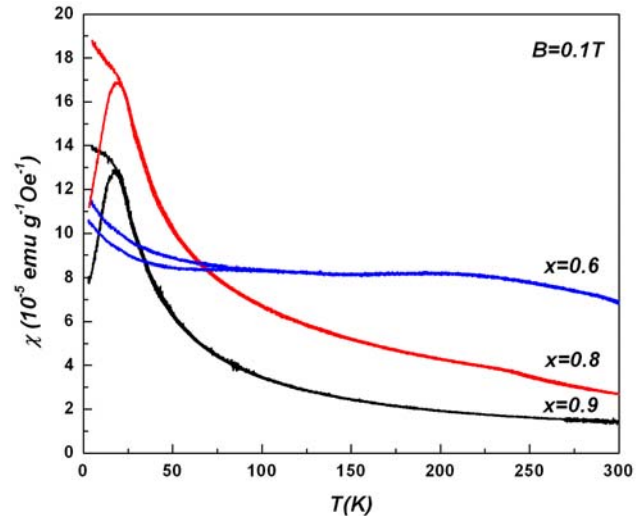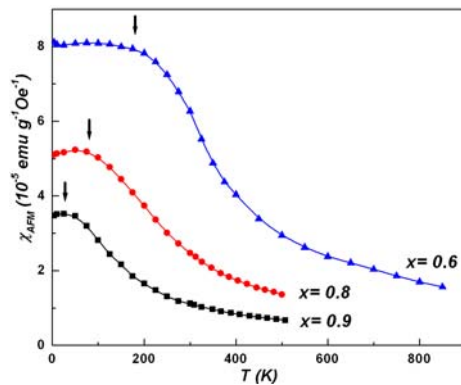

Fig. 4.11. The temperature dependence of the magnetic susceptibility χ_{AFM} of $Mn_{1-x}Al_xNi$ alloys. The arrows indicate the Néel temperatures.
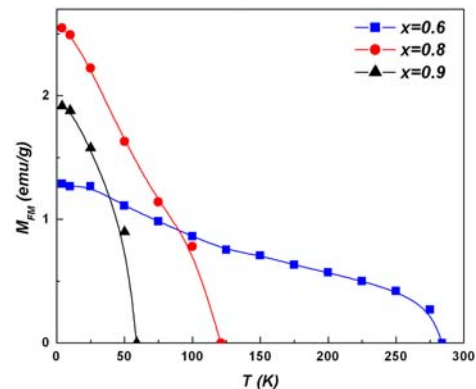

Fig. 4.12. The temperature dependence of the magnetization M_{FM} for $Mn_{1-x}Al_xNi$ alloys.

respectively T_N, we have used the Honda-Arrot plot for each temperature.

In Figs. 4.11 and 4.12 are shown the temperature dependence of the as determined susceptibility χ_{AFM} and magnetization M_{FM}, respectively. The curves $\chi_{AFM}(T)$ present a downward at certain temperatures, referred as the Néel temperatures. At about the same temperatures $T \approx T_N$, the curves $M_{FM}(T)$ show a small anomaly in the magnetization of the ferromagnetic component, due to the pinning effect. The Curie temperatures T_C have been determined in the molecular field approximation from the $M_{FM}^2(T)$ dependence. The as determined transition temperatures are given in Table 4.1.

The thermal variation of the reciprocal magnetic susceptibility for the investigated alloys in the high temperature range is shown in Fig. 4.13. The experimental data fit a Curie-Weiss law with a small additional temperature-independent term χ_0.

The values of the effective magnetic moments μ_{eff} and of the paramagnetic Curie temperatures θ are given in Table 4.1. The Ni 3d band for $x \geq 0.5$ is almost filed. This assumption is confirmed by the very small intensity of the Ni 2p and valence band satellite. The contribution of the Ni atoms to the total effective magnetic moment is negligible, so the measured effective magnetic moment may be attributed only to the Mn atoms. The effective magnetic moments per Mn atom have approximately the same value, corresponding to a spin $S \cong 2$,

Fig.4.13. Reciprocal susceptibility versus temperature of $Mn_{1-x}Al_xNi$ alloys.

like in the parent compound MnNi, showing that the Mn 3d band is not affected by alloying, suggesting that the hybridization between the Mn 3d states and the Al 3sp states is very small. The paramagnetic Curie temperatures θ are much lower than the Curie temperatures T_C. This is due to the contribution of antiferromagnetic part in the measured magnetic susceptibility, which has a negative θ value, and consequently an averaged paramagnetic Curie temperature is observed. The relative proportion of the ferromagnetic and antiferromagnetic parts in the samples is also reflected in the difference between the Curie temperatures T_C and paramagnetic Curie temperatures θ as a function of the Al content. This difference decreases with Al concentration, confirming the decrease of the antiferromagnetic component at lower Mn concentrations.
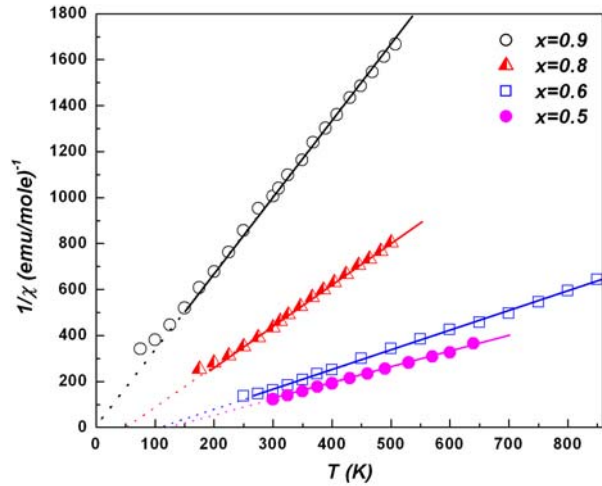
Table. 4.1. Transition temperatures and effective magnetic moments of $Mn_{1-x}Al_xNi$ alloys

x	T_N (K)	T_C (K)	θ (K)	$\mu_{eff}(\mu_B/f.u.)$	$\mu_{eff}(\mu_B/Mn)$
0.5	313*	375*	123	3.44	4.87
0.6	181	284	108	3.07	4.85
0.8	80	121	50	2.21	4.94
0.9	26	59	-3	1.55	4.90

*data taken from [45]

18

Chapter 5
Electronic structure and magnetic properties of $Ni_{1-x}Mn_xAl$ alloys [54-56]

In the previous two chapters it was studied the influence of the substitution of Mn by Al in the ternary system Al-Mn-Ni, on the electronic, crystallographic and magnetic structure, keeping the Ni atomic concentration constant. In the present chapter the Al atomic concentration will remain the same and we will focus on the effect of the substitution of Ni by Mn.

There are no reports about bulk AlMn in a stable phase, but only on $Al_{0.89}Mn_{1.11}$ [57]. In the other side of the concentration range is AlNi, a Pauli paramagnet. Magnetic properties of the $Ni_{1-x}Mn_xAl$ alloys were reported in literature [58], but there are no explanation regarding the relative small values of the measured magnetic moments per atom, their variation with Ni atoms concentration and if Ni brings or not a contribution in the measured magnetic moments.

The aim of this chapter is to explain the magnetic properties of the investigated alloys by correlating the magnetic measurements, in the ordered and paramagnetic state, with XRD and XPS results.

5.1 Structural characterization

Seven samples from the $Ni_{1-x}Mn_xAl$ system (x=0.0, 0.2, 0.3, 0.4, 0.5, 0.6, 0.8) were prepared. XRD measurements were performed on polished surfaces due to the hardness of the samples. The broad character of the peaks indicates the presence of the strains in the samples. X-ray diffraction pattern of $Ni_{1-x}Mn_xAl$ alloys are shown in Fig. 5.1.
All the investigated alloys are single phases with the same CsCl (B2) structure type. The lattice parameter, estimated using the Powder Cell program, increases monotonically with Mn concentration from a=2.875 Å for NiAl to a=2.966 Å for $Ni_{0.2}Mn_{0.8}Al$.

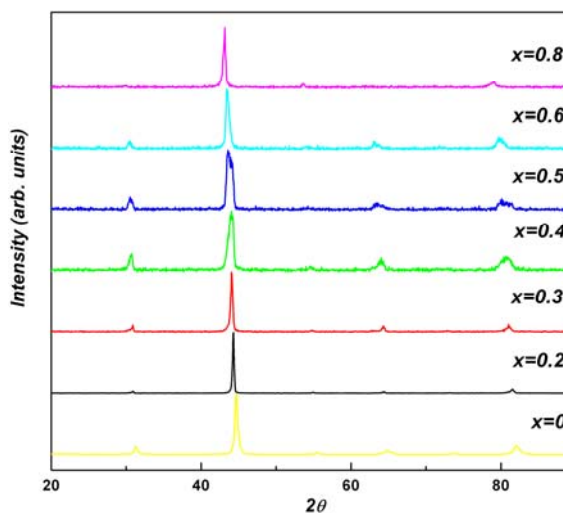*Fig. 5.1. X-ray diffraction pattern of $Ni_{1-x}Mn_xAl$ alloys.*

5.2 XPS Spectra

The XPS valence band spectra of investigated alloys are shown in Fig. 5.2. The maximum of the Ni 3d band is shifted to a BE of 1.8 eV comparing to the value of 0.6 eV in pure metallic Ni [46]. There is also an appreciable hybridization between the Mn 3d and Al 3sp states which leads, according Mn 3s XPS spectra and magnetic measurements, to a partial filling of the Mn 3d band.

The Ni 2p spectra for all investigated alloys are situated at the same BE, but are shifted to higher BE relative to pure metallic Ni. This also confirms the partial filling of Ni 3d band. The first vicinity of Ni atoms in the $Ni_{1-x}Mn_xAl$ alloys does not change by alloying, what explains the lack of the chemical shift in the Ni 2p spectra. The intensity of the Ni 2p satellites in $Ni_{1-x}Mn_xAl$ alloys is drastically reduced (see Fig. 5.3) confirming the partial filling of the Ni 3d band of the investigated alloys, except for x=0 where the satellite structure disappears. This confirms the previous magnetic measurements that have shown that NiAl is a Pauli paramagnet with Ni 3d band completely filled, at room temperature, due to the hybridization with Al 3sp states.
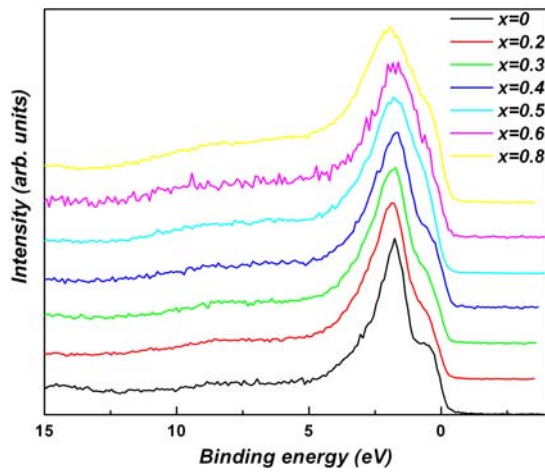
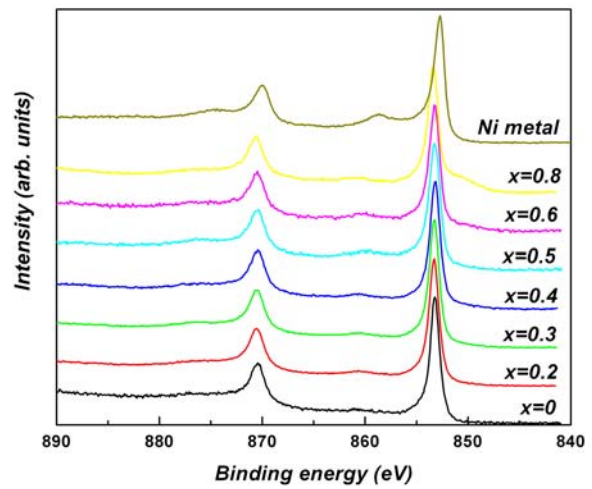*Fig .5.2. XPS valence band spectra of $Ni_{1-x}Mn_xAl$ alloys*

Fig .5.3. Ni 2p XPS spectra of $Ni_{1-x}Mn_xAl$ alloys and pure metallic Ni

The Mn 3s core level spectra show an exchange splitting around 4 eV arising from the exchange interactions between the core hole and the open 3d shell. The exchange splitting in MnNi is about 5.2 eV and the Mn magnetic moment is about 4 μ_B/Mn [40]. The exchange splitting is proportional with the Mn local moment [46]. Fig. 5.4 presents the curve fitting results of $Mn_{0.8}Ni_{0.2}Al$ alloy, after background subtraction, and the similar spectrum of MnNi compound.
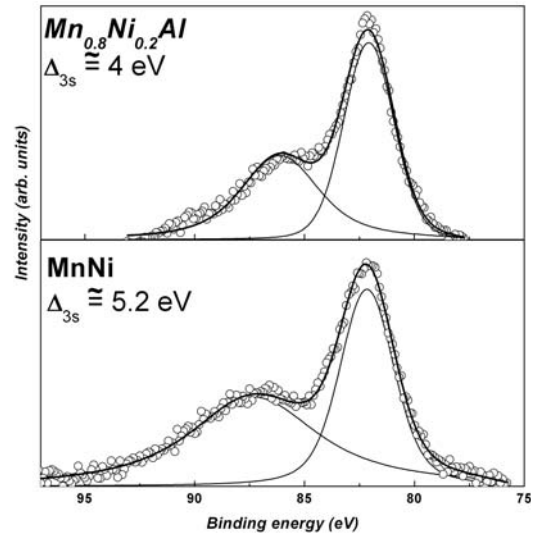

Fig. 5.4. Mn 3s curve fitting results of $Mn_{0.8}Ni_{0.2}Al$ alloy and MnNi compound

5.3 Magnetic measurements

The temperature dependence of the spontaneous magnetization of $Ni_{1-x}Mn_xAl$ alloys is shown in Fig. 5.5.
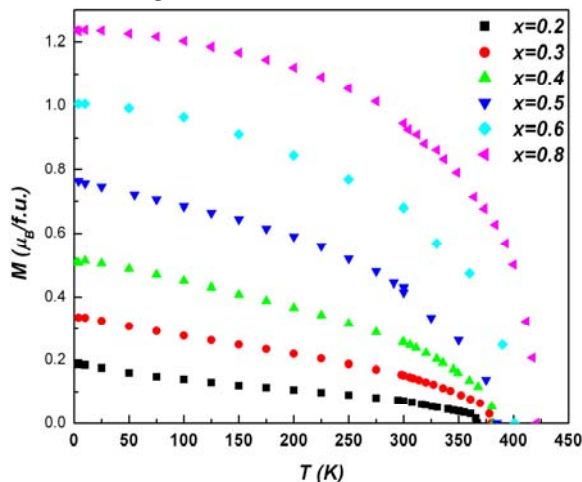

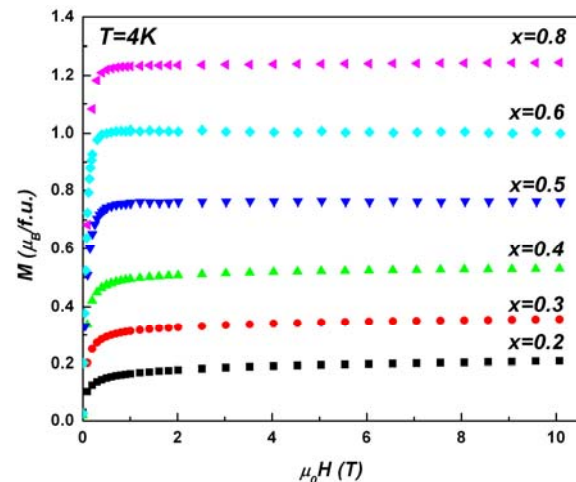*Fig. 5.5. Temperature dependence of spontaneous magnetization of $Ni_{1-x}Mn_xAl$ alloys*

Fig. 5.6. Magnetic field dependence of magnetization at T=4K of $Ni_{1-x}Mn_xAl$ alloys.

The values and variations of magnetization with magnetic field (Fig. 5.6) and temperature suggest that all the investigated alloys have a ferromagnetic behavior, below the corresponding Curie temperatures. The Curie temperatures T_C have been determined in the molecular field approximation from the $M_{FM}^2(T)$ dependence. The values are given in Table 5.1.

The thermal variation of the reciprocal magnetic susceptibility for the investigated alloys in the high temperature range is shown in Fig. 5.7. The experimental data fit a Curie-Weiss law with a small additional temperature-independent term χ_0. The values of the effective magnetic moments μ_{eff} and of the paramagnetic Curie temperatures θ are given in Table 5.1. As one can see from Fig. 5.7, the contribution of χ_0 is more pronounced in the measured magnetic susceptibility for smaller Mn concentrations.

The ratio $\delta = \dfrac{\chi_p^{meas}}{\chi_p^0}$ between the

between the Pauli susceptibilities of d electrons measured and calculated in the free electron approximation is the Stoner enhancement factor which for

Fig.5.7. Reciprocal susceptibility versus temperature of Ni$_{1-x}$Mn$_x$Al alloys. In the inset is given the temperature dependence of magnetic susceptibility of NiAl [59]

NiAl has the value $\delta = 1.8$. This value shows that NiAl is exchange-enhanced Pauli paramagnet, suggesting that also the Ni$_{1-x}$Mn$_x$Al alloys could be exchange-enhanced Pauli paramagnets, which are correctly treaded in the self-consistent renormalization (SCR) theory of spin fluctuations [35].
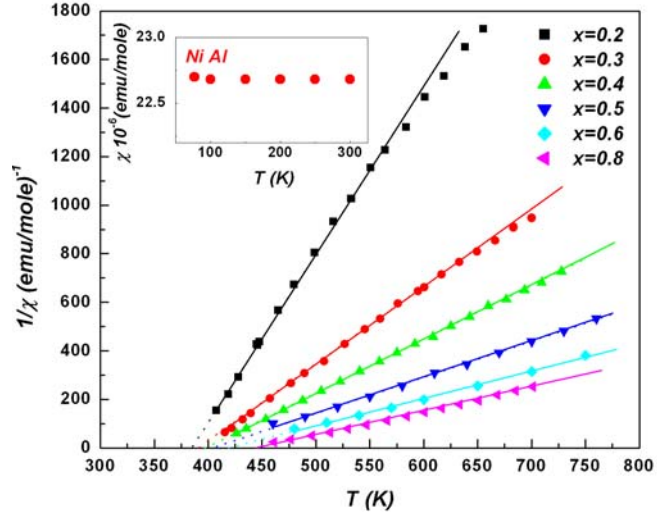
Table 5.1. The magnetic moments in the ordered (μ) and paramagnetic state (μ_{eff}), the Curie (T_C) and paramagnetic Curie (θ) temperatures and the lattice constants (a) of the Ni$_{1-x}$Mn$_x$Al alloys.

	μ (μ_B/f.u.)	μ_{eff} (μ_B/f.u.)	T_C (K)	θ (K)	a (Å)
x=0					2.8752
x=0.2	0.19	1.06	367	385.7	2.8919
x=0.3	0.34	1.57	379.8	395	2.906
x=0.4	0.51	1.9	381.5	398.8	2.9155
x=0.5	0.77	2.32	385	405.5	2.927
x=0.6	1.01	2.66	401	422.7	2.9356
x=0.8	1.24	2.9	420.8	445.9	2.9664

T_C and θ increase monotonically with Mn concentration in good agreement with the theory of ferromagnetic materials, T_C being proportional with the number Z of neighboring magnetic atoms [60]. Comparing the intensity of the Ni 2p and valence band satellites in this system with the similar ones in the previous system Mn$_{1-x}$Al$_x$Ni, one may conclude that also in Ni$_{1-x}$Mn$_x$Al alloys the Anderson condition of the existence of a local moment on Ni sites in the ordered state is not fulfilled. So, the measured magnetic moments in the ordered state are attributed to Mn atoms only. The values of the Mn spins S_{Mn} (see Table 5.2) were obtained from the relation $\mu_{Mn} = 2 S_{Mn}\mu_B$. Using these values, the effective Mn magnetic moments are calculated

($\mu_{eff}^{Mn} = 2\sqrt{S_{Mn}(S_{Mn}+1)}\mu_B$). In the paramagnetic region we have to consider the contribution of Ni magnetic moments, induced by temperature, to the magnetic susceptibility (the Ni 3d band is not completely filled). The Ni contribution to the effective magnetic moment was calculated ($\mu_{f.u.}^2 = x\mu_{Mn}^2 + y\mu_{Ni}^2$, x and y are the molar fraction of Mn and Ni, respectively). The Ni effective magnetic moment has reasonable values for x≤0.4, comparable with the values on Ni sites in other spin fluctuation systems [61, 62]. For x>0.4 the calculated Ni effective magnetic moments are too large; this suggests that not all the Mn atoms moments are orientated in the same direction and is possible to have antiferromagnetic Mn-Mn pairs. The probability of the apparition of Mn-Mn antiferromagnetic pairs increases with Mn concentrations.

The strong Mn 3d - Al 3sp hybridization is due to the high number of Al atoms in the Mn first vicinity, namely 8 Al atoms at ~2.5 Å. This explains the small values of the Mn magnetic moments in $Ni_{1-x}Mn_xAl$ alloys comparing to MnNi. The Mn magnetic moment in the ordered state increases with Mn concentration, except for the x=0.8 alloy. This variation can be associated with the increase of the lattice parameter which leads to a decreasing in the Mn 3d - Al 3sp hybridization degree. But

Table 5.2. The magnetic moments and spin of Mn atoms in the ordered state and the calculated Mn effective magnetic moments of the $Ni_{1-x}Mn_xAl$ alloys.

	μ_{ord}^{Mn}	S_{Mn}	μ_{eff}^{Mn}
x=0.2	0.95	0.48	1.69
x=0.3	1.13	0.57	1.89
x=0.4	1.28	0.64	2.05
x=0.5	1.54	0.77	2.33
x=0.6	1.68	0.84	2.49
x=0.8	1.55	0.78	2.36

together with the Mn concentration, increases also the probability of the Mn-Mn antiferromagnetic pairs formation, so that a number of Mn magnetic moments do not contribute to the magnetization. These two phenomena influence the value of the measured magnetic moments.

It is well known that Mn-Mn interaction is antiferromagnetic when the distance is smaller than ~2.9 Å [63], comparable with the lattice constant in $Ni_{1-x}Mn_xAl$ alloys. For larger values the coupling is ferromagnetic. In these alloys there are two possibilities for the appearance of antiferromagnetic Mn-Mn pairs:

- There are two Mn atoms in the centre of near neighbour cells and lattice parameter is smaller than 2.9 Å;
- A crystallographic disorder appears: Mn and Al atoms switch places, thus the Mn-Mn distance became ~2.5 Å.

Chapter 6
Electronic structure and magnetic properties of $Ni_{0.7-x}Al_xMn_{0.3}$ alloys [64]

In the last three chapters it was presented the effect of the substitution of Mn by Al atoms and Ni by Mn atoms in the electronic, crystallographic and magnetic structure, keeping the Ni and respective Al atomic concentration constant. To have a complete picture of the Al-Mn-Ni system in this chapter the Mn atomic concentration will remain the same and the substitution effect of Ni by Al atoms will be studied.

6.1 Structural characterization

Seven samples from the $Ni_{0.7-x}Al_xMn_{0.3}$ system (x=0.0, 0.1, 0.2, 0.3, 0.4, 0.5, 0.7) were prepared. XRD measurements were performed on polished surfaces due to the hardness of the samples. X-ray diffraction pattern of $Ni_{0.7-x}Al_xMn_{0.3}$ alloys are shown in Fig. 6.1. The broad character of the peaks indicates the presence of the strains in the samples.

All the investigated alloys are single phases except for $Al_{0.7}Mn_{0.3}$ and $Ni_{0.5}Al_{0.2}Mn_{0.3}$ alloys. XRD measurements revealed a change in the crystallographic structure around x = 0.2 from $AuCu_3$ to CsCl (B2) structure type. $Ni_{0.5}Al_{0.2}Mn_{0.3}$ appears as a mixture of these two structures. The results only from the single phase alloys are presented in the following pages.
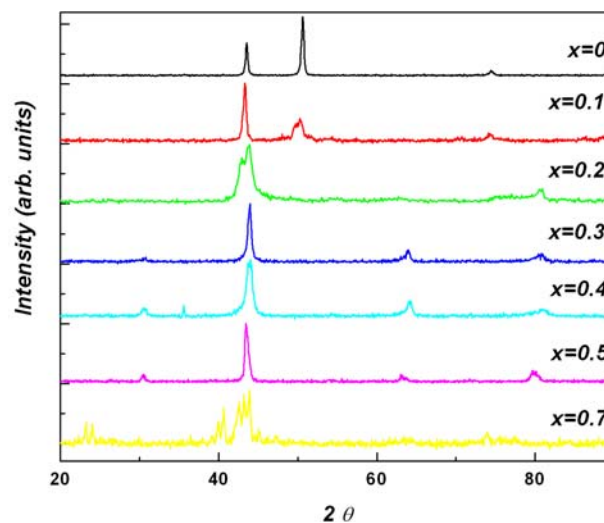

Fig. 6.1. X-ray diffraction pattern of $Ni_{0.7-x}Al_xMn_{0.3}$ alloys

6.2 XPS spectra

XPS valence band spectra of the $Ni_{0.7-x}Al_xMn_{0.3}$ alloys are shown in Fig. 6.2. The Mn 3d states are concentrated at the bottom of the valence band in the region around 3 eV binding energy and became more visible at low Ni concentrations. The valence band centroids are shifted towards higher binding energies and the density of states at Fermi level decreases as the Al concentration increases, suggesting a gradual filling of the Ni 3d band due to hybridization of the Al 3sp and Ni 3d states. In d-band metals and alloys the 3d states are shifted gradually to higher binding energy with the increase in the d-state occupancy and consequently a decrease in the density of states at the Fermi level occurs.
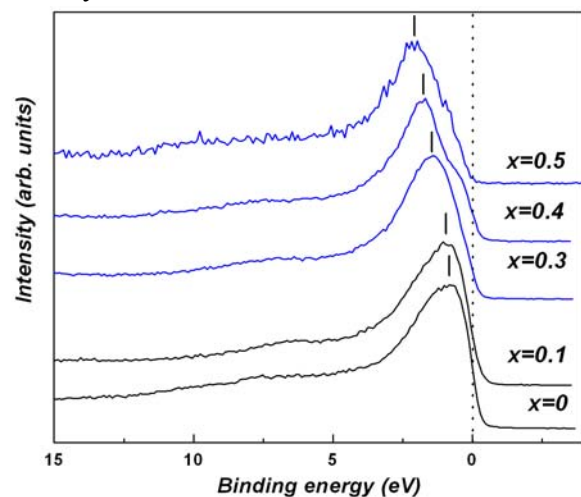

Fig. 6.2. XPS valence band spectra of $Ni_{0.7-x}Al_xMn_{0.3}$ alloys.

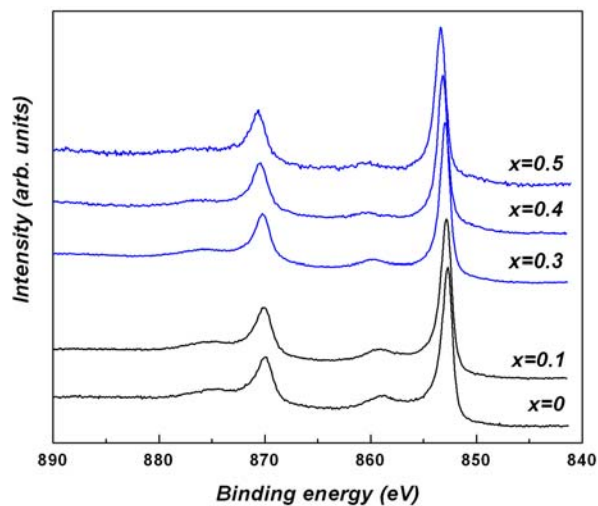Fig .6.3. Ni 2p XPS spectra of $Ni_{0.7-x}Al_xMn_{0.3}$ alloys

The Ni 2p core-level spectra of $Ni_{0.7-x}Al_xMn_{0.3}$ alloys are shown in Fig. 6.3. As the Al concentration increases, the Ni 2p core-level lines are shifted to higher binding energy. These small chemical shifts are due to the change in the filling degree of the Ni 3d band, which leads to

an increase in the electronic density around the Ni 2p shell. The 6 eV satellite structure intensity decreases as the Al content increases, confirming the gradual filling of the Ni 3d band. The presence of the satellite structures suggests that Ni atoms could carry a small magnetic moment.

There is an overlapping between Mn2p XPS line and Ni $L_2M_{23}M_{45}$ Auger line (Fig. 6.4). The observed spin orbit splitting, which can be identified in the distance between the two centers of energy of the Mn $2p_{3/2}$ and $2p_{1/2}$ state is $\Delta_{so} \approx 11.5$ eV.
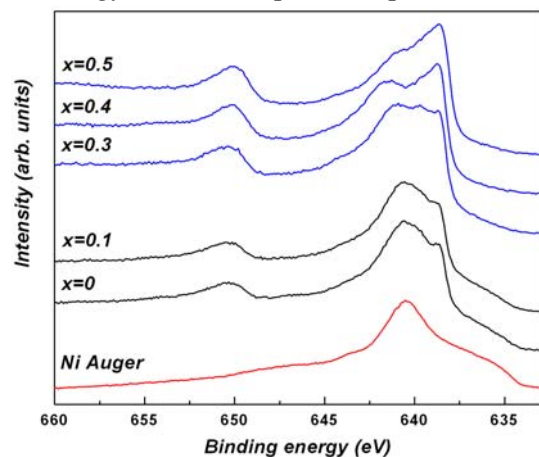

Fig .6.4. Mn 2p XPS spectra of $Ni_{0.7-x}Al_xMn_{0.3}$ alloys and Ni Auger line
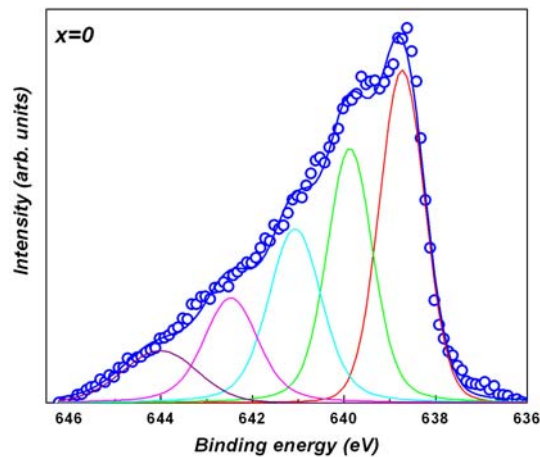
Fig. 6.5. Mn $2p_{3/2}$ curve fitting results of $Ni_{0.7}Mn_{0.3}$ alloy

We have also fitted the Mn $2p_{3/2}$ core-level spectra for some of the investigated alloys. The curve fitting results for $Ni_{0.7}Mn_{0.3}$ alloy is given in Fig. 6.5, with the mean energy separation $\Delta_{ex} \approx 1.1$ eV, comparable with the values observed in other Ni alloys [65]. This gives direct evidence of the existence of local moments confined on Mn sites.

6.3 Magnetic measurements

The temperature dependence of magnetic susceptibility of $Ni_{0.7}Mn_{0.3}$ and $Ni_{0.4}Al_{0.3}Mn_{0.3}$ alloys is given in Fig. 6.6. The susceptibility presents a maximum, specific for antiferromagnetic materials, which corresponds to Néel temperature. The values of the transition temperature are $T_N \approx 150K$ and $T_N \approx 125K$ for $Ni_{0.7}Mn_{0.3}$ and $Ni_{0.4}Al_{0.3}Mn_{0.3}$, respectively.
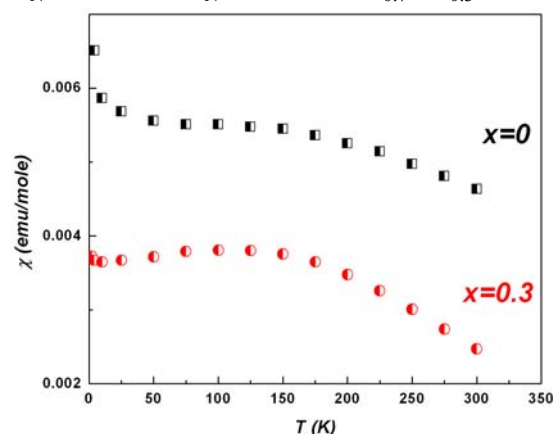

Fig. 6.6. The temperature dependence of magnetic susceptibility of $Ni_{0.7}Mn_{0.3}$ and $Ni_{0.4}Al_{0.3}Mn_{0.3}$ alloys
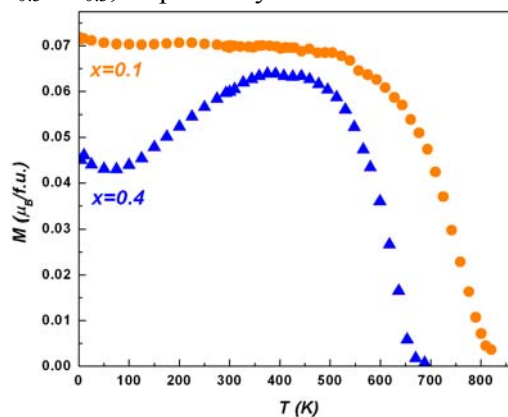
Fig. 6.7. The temperature dependence of the spontaneous magnetization of $Ni_{0.6}Al_{0.1}Mn_{0.3}$ and $Ni_{0.3}Al_{0.4}Mn_{0.3}$ alloys

The increase of the magnetic susceptibility at very low temperatures could be due to some ferromagnetic impurity or a conical antiferromagnetic structure, which has a ferromagnetic component. This feature was also observed in the Chapter 4.

The spontaneous magnetization as a function of temperature is given in Fig. 6.7 for $Ni_{0.6}Al_{0.1}Mn_{0.3}$ and $Ni_{0.3}Al_{0.4}Mn_{0.3}$ alloys. The small values of spontaneous magnetization suggest a ferrimagnetic behavior of these two alloys.

Fig. 6.8 shows the temperature dependence of the reciprocal susceptibility of $Ni_{0.6}Al_{0.1}Mn_{0.3}$ and $Ni_{0.3}Al_{0.4}Mn_{0.3}$ alloys in the paramagnetic state. The reciprocal of magnetic susceptibility follows a Néel-type hyperbolic law, specific to ferrimagnetic materials. Usually for ferromagnetic materials, the high temperature asymptote to the hyperbola has a Curie-Weiss form. Unfortunately, for these two alloys, because the transition temperature is very high and the instrumentation upper limit temperature was around 900K, the asymptote to the hyperbola was not reached.
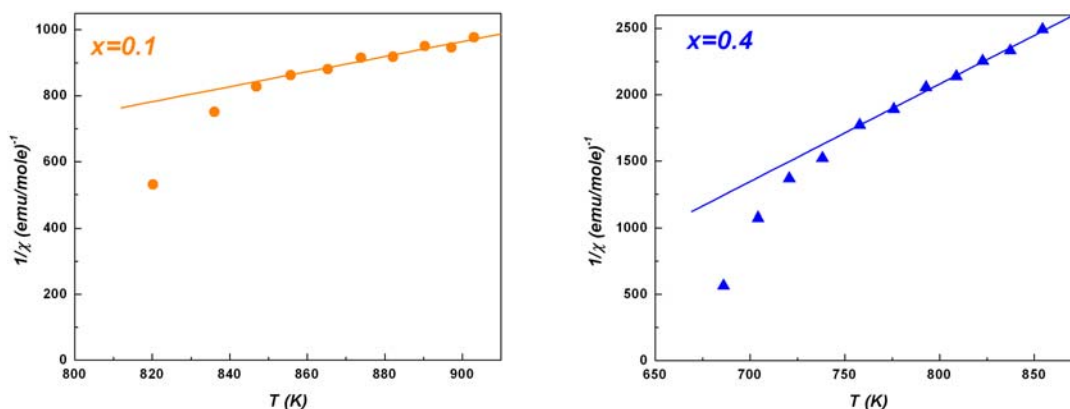

Fig. 6.8. The temperature dependence of the reciprocal susceptibility of $Ni_{0.6}Al_{0.1}Mn_{0.3}$ and $Ni_{0.3}Al_{0.4}Mn_{0.3}$ alloys

The Curie temperatures T_C have been determined in the molecular field approximation from the $M_{FM}^2(T)$ dependence and have the values 780.5K and 645K for $Ni_{0.6}Al_{0.1}Mn_{0.3}$ and $Ni_{0.3}Al_{0.4}Mn_{0.3}$, respectively.

The values and the variation of the magnetization with the temperature (Fig. 6.9a) suggest a ferromagnetic behavior of $Ni_{0.2}Al_{0.5}Mn_{0.3}$ alloy. The ferromagnetic Curie temperature, determined in the same way like above, has the value $T_C=400K$. The reciprocal susceptibility as a function of temperature for $Ni_{0.2}Al_{0.5}Mn_{0.3}$ alloy is presented in Fig. 6.9b and confirms the ferromagnetic behavior. The experimental data fit a Curie-Weiss law.
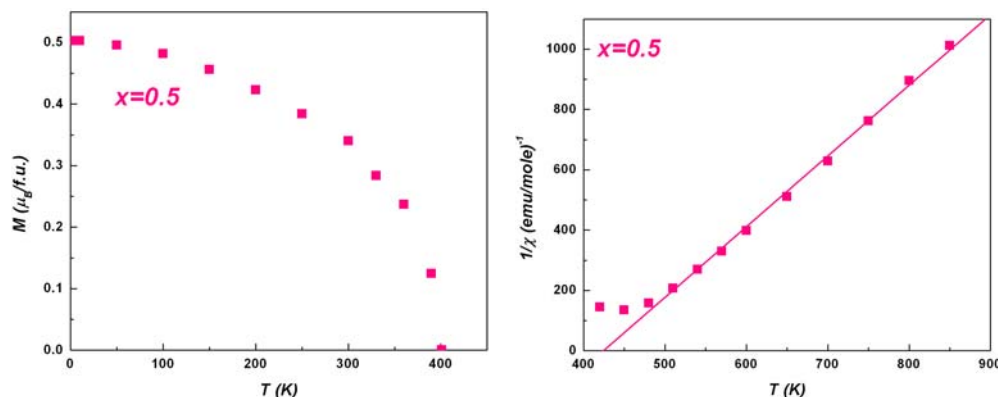
Fig. 6.9. The spontaneous magnetization (a), and the reciprocal magnetic susceptibility (b) as a function of temperature of $Ni_{0.2}Al_{0.5}Mn_{0.3}$ alloy

The magnetic behavior of $Ni_{0.7-x}Al_xMn_{0.3}$ alloys is illustrated in Fig. 6.10. We have seen in the Chapter 3 that in the ordered $AuCu_3$ structure type, Mn and Al atoms occupy the 1a position and Ni atoms are situated in 3c position. In this case the coupling between the Mn atoms

is ferromagnetic ($d_{Mn-Mn} > 2.9 A°$). In the crystallographically disordered alloys a number of Mn atoms occupy the 3c positions and generate antiferromagnetic Mn-Mn pairs with the Mn atoms from their firs vicinity situated in 1a or 3c positions ($d_{Mn-Mn} < 2.9 A°$). In $AuCu_3$ structure type 25% of atoms will occupy the 1a position and 75% the 3c position. On can see that in $Ni_{0.7}Mn_{0.3}$ alloy even if the disorder degree is considered to be zero, a number of Mn atoms will be forced to take the 3c position and to form Mn-Mn antiferromagnetic pairs. Furthermore, at this Mn concentration the alloy is crystallographically disordered (see Chapter 3), with a disorder degree very high. This explain the magnetic measurements results, which shown that $Ni_{0.7}Mn_{0.3}$ alloy has antiferromagnetic behavior.

In the Chapter 3 we have also seen that Al atoms play an important role in the stability of the crystallographically ordered structures, and the probability of the apparition of antiferromagnetic Mn-Mn pair decrease with the increase of Al concentration. This explains why $Ni_{0.6}Al_{0.1}Mn_{0.3}$ alloy has a ferrimagnetic behavior.
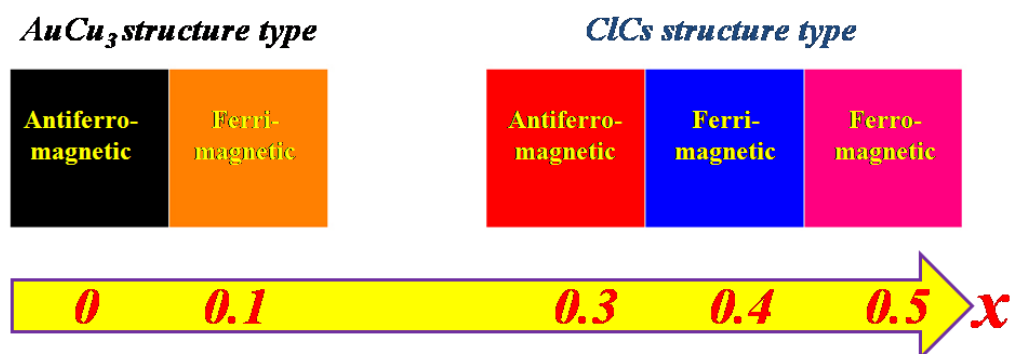

Fig. 6.10. The magnetic behavior of $Ni_{0.7-x}Al_xMn_{0.3}$ alloys

The $Ni_{0.4}Al_{0.3}Mn_{0.3}$ alloy has the lattice parameter a≈2.90Å. At this distance the Mn-Mn coupling is antiferromagnetic. The $Ni_{0.3}Al_{0.4}Mn_{0.3}$ alloy has the lattice parameter a little bit larger a≈2.914Å, but seems to be at the limit distance between the AFM and FM coupling. This could be a reason why this alloy has ferrimagnetic behavior. The lattice parameter of the $Ni_{0.2}Al_{0.5}Mn_{0.3}$ alloy is larger (a≈2.94) and it has a ferromagnetic behavior. This means that at this distance the coupling between the Mn atoms is parallel.

Conclusions

The main idea of the thesis was to see how one can change the crystallographic structure type, the electronic structure, the values of the magnetic moments and the sign of the interactions between the local magnetic moments by changing the atomic concentration of the constituent atoms in the ternary system Al-Mn-Ni.

The magnetic properties of the investigated alloys and compounds are strongly correlated with their crystallographic properties and reflect the changes in the first vicinity and in the distances between the 3d atoms. By changing the stoichiometry one can change the crystallographic structure type ($Mn_{1-x}Al_xNi$ and $Ni_{0.7-x}Al_xMn_{0.3}$ systems), but even if the crystallographic structure remains the same ($Mn_{1-x}Al_xNi_3$ and $Ni_{1-x}Mn_xAl$) the variation in the lattice parameters leads to changes in the coupling between the magnetic moments of 3d elements.

Some of the Al-Mn-Ni alloys are crystallographically disordered, but the crystallographic disorder degree decreases quickly with the increase of Al concentration. Aluminum plays an

important role in stabilizing the crystallographic ordered structure in $Mn_{1-x}Al_xNi_3$ alloys. The same effect was observed for $Ni_{0.7-x}Al_xMn_{0.3}$ in the small range of Al concentrations.

XPS spectra and magnetic measurements pointed out the existence of local magnetic moments confined to the Mn sites for all Mn-Ni-Al alloys and compounds.

The hybridization between 3d Ni and 3sp Al states leads to a partial or complete filling of Ni 3d band, as indicated by XPS core level and valence band spectra.

XPS and magnetic measurements evidenced that Mn 3d band in $Mn_{1-x}Al_xNi_3$ and $Mn_{1-x}Al_xNi$ systems is not affected by hybridization with Al 3sp states while in $Ni_{1-x}Mn_xAl$ and $Ni_{0.7-x}Al_xMn_{0.3}$ systems Mn 3d band is strongly affected. This depends again on the interatomic distances.

XPS spectra suggest that Ni atoms could carry small magnetic moments in almost all the investigated alloys but, the Anderson condition for the existence of a local magnetic moment at Ni sites, in the ordered magnetic state, is fulfilled only for $Mn_{1-x}Al_xNi_3$ alloys. Ni atoms bring their contribution to the effective magnetic moment in the paramagnetic state. In many cases their contribution is small but for some of the investigated alloys temperature induced spin fluctuations at Ni sites were evidenced.

Magnetic measurements revealed different types of magnetic ordering: ferromagnetic, ferrimagnetic, antiferromagnetic and in some of the investigated alloys coexistence between antiferromagnetism and ferromagnetism was evidenced. By changing the stoichiometry was possible to pass from one type of magnetic ordering to another. A very good example is the $Ni_{0.7-x}Al_xMn_{0.3}$ system, where a transition from antiferromagnetism to ferromagnetism through an intermediate ferrimagnetic phase was evidenced once the Al concentration increases.

The profound understanding of the magnetic phenomena and the correct interpretation of the magnetic properties of the alloys and intermetallic compounds based on transition elements can be achieved only through the correlation of obtained data from XPS, XRD and magnetic measurements, corroborated with the band structure calculations.

Selected references

[1] P.O.M. Dirac, Proc. Roy. Soc. Lond. A 123 (1929) 714-733
[2] J.H. Van Vleck, in "The Theory of Electric and Magnetic Susceptibilities", Oxford University Press, Oxford, 1932
[3] W. Heisenberg, Z. Physik 38 (1926) 411
[4] H.A. Kramers, Physica 1 (1934) 825
[5] P.W. Anderson, Phys. Rev. 115 (1959) 2-13; Solid State Physics 14 (1963) 99
[6] E.C. Stoner, Proc. Roy. Soc. A 165 (1938) 372
[7] J.H. Van Vleck, Rev. Mod. Phys. 25 (1953) 220
[8] P.W. Anderson, Phys. Rev. 124 (1961) 41
[9] J. Friedel, Can. J. Phys. 34 (1956) 1190; Nuovo Cimento Suppl. 7 (1958) 287
[10] S. Alexander and P.W. Anderson, Phys. Rev. 133 (1964) A1594
[11] T. Moriya, Prog. Theor. Phys. 33 (1965) 157; In "Theory of Magnetism in Transition Metals", Proc. Int. School of Phys. Enrico Fermi, vol.37, ed. by W. Marshall, Academic, New York, 1967, p.206
[12] T. Moriya, J. Magn. Magn. Mater. 31-34 (1983) 10
[13] K. Siegbahn, C. Nordling, A. Fahlman, R. Nordberg, K. Hamrin, J. Hedman, G. Johansson, T. Bergmark, S. E. Karlson, I. Lindgren, and B. Lindberg, "ESCA–Atomic, Molecular and Solid State Structure Studied by Means of Electron Spectroscopy", Almquist and Wicksell, Uppsala, 1967
[14] M. Cardona L. Ley (editors), "Photoemission in Solids I", Topics in Applied Physics vol. 26, Berlin: Springer, 1978
[15] S. Hüfner, "Photoelectron Spectroscopy. Principles and Applications", Berlin: Springer, 2003

[16] H. Ebert, in *Electronic Structure and Physical Properties of Solids*, editor: H. Dreysse, Lecture Notes in Physics, vol. 535, Springer, Berlin, 2000, pp. 191; The Munich SPRKKR package, Version 3.6, http://olymp.cup.uni-muenchen.de/ak/ebert/sprkkr

[17] P. Weinberger, *Electron Scattering Theory for Order and Disordered Matter*, University Press, Oxford, 1990.

[18] A.Gonis, *Green Function for Ordered and Disordered Systems*, North-Holland, Amsterdam, 1992.

[19] L. Rednic, R. Pacurariu, **V. Rednic**, L.G. Pascut, V. Pop, M. Neumann, M. Coldea; *X-ray photoelectron spectroscopy and magnetism of AlMnNi$_6$ and Al$_7$Mn$_3$Ni$_{30}$,* J. Optoelectron. Adv. Mat. **9** (2007) 568 – 571.

[20] **V. Rednic**, L. Rednic, M. Coldea, V. Pop, M. Neumann, R. Pacurariu, A. R. Tunyagi, *X-ray Photoelectron Spectroscopy and Magnetism of Mn$_{1-x}$Al$_x$Ni$_3$ Alloys*, Cent. Eur. J. Phys. 6(3) (2008) 434-439.

[21] **V. Rednic**, D. Benea, M. Coldea, V. Pop, L. Rednic and M. Neumann, *KKR calculation of electronic band structure and XPS spectra of Mn$_{1-x}$Al$_x$Ni$_3$ alloys*, sent for publication in J. Optoelectron. Adv. Mat.

[22] M. J. Marcinkowski, R. M. Poliak, Phil. Mag., 8, 1023(1963)

[23] C.G. Shul, M.K. Wilkinson, Phys. Rev. 97**,** 304 (1955)

[24] J. S. Kouvel, C. D. Graham Jr., J. J. Becker, J. Appl. Phys., 29, 518 (1958)

[25] P. J. Kaplan, R. L. Streever, Phys. Rev. B, 2, 3449(1970)

[26] F. R. de Boer, C. J. Schinkel, J. Biesterbos, S. Proost, J. Appl. Phys. 40, 1049(1969)

[27] Ul-Haq and J.G. Booth, J. Magn. Magn. Mat. 62, 256 (1986)

[28] T. Shinohara, T. Takasugi, H. Yamauchi, T. Kamiyama, H. Yamamoto, O. Izumi, J. Magn. Magn. Mat. 53, L1 (1985)

[29] W. B. Pearson, A handbook of Lattice Spacings and Structures of Metals and Alloys, (Pergamon Press, New York, 1958)

[30] J. Yeh, I. Lindau, At. Data Nucl. Tables 32,1(1958)

[31] Y. Kurtulus and R. Dronskowski, J. Sol. State Chem., 176, 390 (2003)

[32] R. Y. Umetsu, K. Fukamichi, A. Sakuma, J. Magn. Magn. Mat. 239, 530(2002)

[33] S. Plogmann, T. Schlatholter, J. Braun, M. Neumann, Yu. Yarmoshenko, M. V. Yabloskikh, E. I. Shreder, E. Z. Kurmaev, Phys. Rev. B, 60(1999)

[34] E.Burzo, N.Bucur, P.Vlaic and **V.Rednic,** *J. Phys.: Condens. Matter* **20** (2008) 7

[35] T. Moriya, Spin Fluctuations in Itinerant Electron Magnetism, (Springer-Verlag, Berlin, 1985)

[36] J. W. Cable, E. O. Wollan, W. C. Koehler, H. R. Child, Phys. Rev. 128, 2118 (1962)

[37] T. Busgen, J. Feydt, R. Hassdorf, S. Thienhaus, M. Moske, Phys. Rev. B 70, 014111(2004)

[38] K. Kneller, in Ferromagnetismus, (Springer-Verlag, Berlin, 1962) 150

[39] **V. Rednic**, M. Coldea, S. K. Mendiratta, M. Valente, V. Pop, M. Neumann and L. Rednic, *X-ray Photoelectron Spectroscopy and Magnetism of Mn$_{1-x}$Al$_x$Ni Alloys*, J. Mag. Mag. Mat 321 (2009) 3415–3421

[40] L. Pal et al, J. Appl. Phys. **39** (1968) 538

[41] G. Bayreuther, in Magnetische Schicht-systeme, 30. Ferienkurs des Instituts für Festkörperforschung, Julich, 1999

[42] Ch. Müller, H. Wonn, W. Blau, P. Ziesche and V. P. Krivitshii, Phys Stat Sol. B 95 (1979) 215

[43] Lluis Manosa et al, J. Appl. Phys., **93**, (2003) 8498

[44] S. Morito, T. Kakeshita, K. Hirata, K. Otsuka, Acta mater. **46** (1998) 5377

[45] M. Acet, E. Duman, E. F. Wassermann, L. Manosa and A. Planes, J. Appl. Phys. **92** (2002) 3867

[46] S. Hüfner, Photoelectron Spectroscopy Principles and Applications, Springer-Verlag, Berlin (1995), p. 89

[47] **V. Rednic**, M. Coldea, L. Rednic, L. G. Pascut, N. Aldea, S. Pintea and M. Neumann, Journal of Physics: Conf Series, **182** (2009) 012077

[48] A. Sakuma, J. Magn. Magn. Mat. **187** (1998) 105

[49] A. Kjekshus, R. Mollebud, A. F. Andresen, and W. B. Pearson, Philos. Mag. **16** (1967) 1063

[50] K. H. J. Buschow, J. F. Fast, A. M. Van Diepen and H. W. de Wijn, Phys Stat Sol. **24** (1967) 715

[51] R. Harris, M. Plischke, M. J. Zuckermann, Phys. Rev. Lett. **31**(1973) 160

[52] T. Hori, H. Shiraishi, Y. Nakagawa, J. Appl. Phys. **79** (1996) 6633

[53] K. R. A. Ziebeck, P. J. Webster, J. Phys. F: Met. Phys. **5**(1975) 1756

[54] **V. Rednic**, R. Pacurariu, L. Rednic, V. Pop, M. Neumann, M. Coldea; *Magnetism and X-ray Photoelectron Spectroscopy of AlNi$_{1-x}$Mn$_x$ Alloys;* Studia Universitatis Babes Bolyai, Physica, LI, **2** (2006) 20 – 26.

[55] **V. Rednic**, R. Pacurariu, L.G. Pascut, V. Pop, M. Neumann, and M. Coldea; *X-Ray Photoelectron Spectroscopy and Magnetism of Al$_2$MnNi and Al$_5$Mn$_3$Ni$_2$,* Moldavian Journal of the Physical Sciences, vol. **6** (2007) 86-91.

28

[56] **V. Rednic**, M. Coldea, O. Isnard, M. Neumann and L. Rednic, *Electronic structure and magnetic properties of $Ni_{1-x}Mn_xAl$ alloys*, prepared for publication in Phys. Stat. Sol. B.

[57] P. B. Braun, J. A. Goedkoop, Acta Cryst. 16 (1963) 737

[58] Y. Hara, R. C. O' Handley, N. J. Grant, J. Magn. Magn. Mater. 54-57 (1986) 1077-1078

[59] M. B. Brodsky and J. O. Brittain, J. Appl Phys, **40** (1969) 3615

[60] Ch. Kittel, *Introduction to Solid State Physics*, Wiley, New York (1975)

[61] E. Burzo, E. Gratz and V. Pop, J. Magn. Magn. Mater., **123**, (1993) 159

[62] M. Coldea, D. Andreica, M. Bitu and V. Crisan, J. Magn. Magn. Mater., 157/158 (1996) 627

[63] A. Kjekshus, R. Mollebud, A.F. Andresen, and W.B. Pearson, Phil. Mag. 16 (1967) 1063

[64] **V. Rednic**, M. Coldea, O. Isnard, M. Neumann and L. Rednic, *Crystallographic and electronic structure of $Ni_{0.7-x}Al_xMn_{0.3}$ alloys,* accepted for publication in Studia Universitatis Babes-Bolyai, Physica

[65] R. Pacurariu, **V. Rednic**, M. Coldea, D. Benea, V. Pop, O. Isnard, and M. Neumann, Phys. stat. sol. (b), **246** (2009) 50-55